RSC Advances

PAPER

View Article Online
View Journal | View Issue

Cite this: *RSC Adv.*, 2025, **15**, 12876

Fabrication of cell-laden hydrogel microcapsules of alginate and chitin fibrils using divalent and trivalent metal ions

Thakur Sapkota,[ab] Sita Shrestha,[b] Bishnu P. Regmi [c] and Narayan Bhattarai *[ab]

Nanofiber-embedded 3D hydrogel constructs have garnered significant attention due to their versatile applications in drug delivery, cell therapy, tissue engineering, and regenerative medicine. These constructs are especially prized for their capacity to mimic the composition of the extracellular matrix (ECM) found in living tissues and organs. The unique chemical and mechanical properties of hydrogel microcapsules have made them particularly notable among various biomaterial constructs for their effectiveness in cell encapsulation, which aims to improve cell growth and proliferation. In this study, we developed alginate hydrogel microcapsules embedded with chitin nanofibrils, using divalent calcium ions and trivalent iron ions as crosslinking agents. An electrostatic encapsulation technique was utilized to create microcapsules with diameters ranging from 200–500 μm, and their physicochemical properties, rheological properties, size, and mechanical stability were evaluated. The rheological analysis demonstrated that the Fe^{3+} crosslinked hydrogel (AF0) and Fe^{3+}/Ca^{2+} cross-linked hydrogel (AFC) have higher storage modulus than the Ca^{2+} crosslinked hydrogel (AC0). Additionally, FTIR analyses of AF0 and AFC demonstrated a broader –O–H stretching peak compared to that of AC0, suggesting that more hydroxyl groups of alginate chains are involved in crosslinking with ferric ions exhibiting extended mechanical stability compared to those crosslinked with calcium ions under *in vitro* physiological conditions. We also investigated the cellular responses to the composite hydrogels crosslinked with these divalent and trivalent metal ions through *in vitro* studies involving the seeding and encapsulation of NIH/3T3 fibroblast cells. Remarkably, both types of crosslinked microcapsules maintained excellent cell viability for up to 5 days. Our *in vitro* scratch assay demonstrated that media extracted from AF0 microcapsules facilitated faster wound closure compared to that extracted from AC0, suggesting that hydrogels crosslinked with Fe^{3+} ions promote enhanced cellular proliferation. These results suggest that calcium and ferric ion crosslinked alginate–chitin composite microcapsules provide a promising platform for developing 3D hydrogel constructs suitable for various biomedical applications, including wound healing models, tissue engineering, and drug toxicity testing.

Received 27th February 2025
Accepted 16th April 2025

DOI: 10.1039/d5ra01397f

rsc.li/rsc-advances

Introduction

Tissue engineering, regenerative medicine, and drug delivery paradigms have been revolutionized by the introduction of biopolymer-derived architectures, such as hydrogels, micro- and nanofibrils, micro- and nanoparticles, films, and porous scaffolds. These engineered structures play a vital role *in vivo* due to their ability to restore the native extracellular matrix (ECM), provide controlled microenvironments, and protect cells from external factors, such as shear stress from the surrounding medium and the host immune system.[1,2] Cell encapsulation in hydrogel-based structures provides an optimal environment for cell survival and maintains maximum cellular functions due to the ability of hydrogels to facilitate the exchange of metabolites, nutrients, and oxygen. Among these structures, fiber-integrated composite hydrogel microcapsules and microbeads are particularly effective in cell encapsulations and therapies as well as in tissue engineering applications due to their softness, porosity, fibrous construct, and cell attachment moieties, which facilitate cell growth, proliferation, and differentiation.[3,4]

Various biopolymers have been utilized for construction of appropriate hydrogel microcapsules and microbeads. The biopolymers utilized to construct hydrogel structures are classified as synthetic, such as polyethylene glycol (PEG), polycaprolactone (PCL),[5] poly(vinyl alcohol) (PVA), 2-hydroxyethyl methacrylate (HEMA),[6] and polyglycerol sebacate-*co*-polyethylene glycol (PGS-*co*-PEG),[7] and natural polymers, such as

[a]*Department of Applied Science and Technology, North Carolina A&T State University, Greensboro, NC, 27411, USA*
[b]*Department of Chemical, Biological, and Bioengineering, North Carolina A&T State University, Greensboro, NC, 27411, USA. E-mail: nbhattar@ncat.edu*
[c]*Department of Chemistry, Florida Agricultural and Mechanical University, Tallahassee, FL 32307, USA*

alginate, chitin, gelatin, hyaluronic acid, and collagen.[8,9] Synthetic polymers are valued for their tunable physiochemical properties, higher mechanical stability, and slow degradation under physiological conditions, making them suitable for various biomedical applications.[10,11]

Synthetic polymer constructs face challenges in cell culture and tissue engineering applications due to a lack of cell binding moieties, potential autoimmune rejection, and requiring complex chemical reaction while modifying their physical and chemical properties.[12,13] Compared to synthetic polymers, natural biopolymers possess unique features, such as non-immunogenicity, biocompatibility, and biodegradability[14,15] and hence they have been widely used in biomedical applications. Alginate, a natural heteropolysaccharide composed of β-D-mannuronic acid (M) and α-L-guluronic acid (G) linked through glycosidic bonds,[16] is extensively used for the encapsulation of cells and biomolecules because of its proven biocompatibility, cost-effectiveness, ease of gelation under physiological conditions in the presence of divalent and trivalent cations,[17,18] and convenience in sterilization and storage. Rapid gelation ability of alginate is crucial for fabricating microspheres that facilitate cell immobilization and protection, making it suitable for cell transplantation and wound healing applications. However, limited mechanical stability, subpar cell adhesion properties,[19] and susceptibility to dissolution from ion exchange with monovalent ions as well as lacking *in vivo* natural degradation restrict its wider use, particularly in cell therapy and tissue engineering. To overcome these limitations, blending alginate with natural and synthetic polymers, incorporating cell adhesion oligopeptides, such as arginine–glycine–aspartate (RGD),[20] and partial oxidation[21] practices have been considered.

One of the natural polymers that has been widely used in biomaterials is chitin polymer, a cationic polysaccharide, due to its proven biological and mechanical properties. In alginate–chitin composite hydrogels, chitin fibrils act as fillers in the hydrogel's void spaces, providing excellent reinforcement to enhance the mechanical strength of alginate hydrogels.[22] The fibrous structure of chitin, like glucosamine glycan of tissue ECM, serves as an essential binding site for cell integrin, thereby facilitating cell attachment. The gelation of alginate–chitin composites is essential for constructing stable hydrogel structures.[23] Various gelation methods, including ionotropic gelation, pH-induced gelation, temperature-induced gelation, and covalent crosslinking, have been utilized.[24–26] Among these methods, ionotropic crosslinking is preferred for cell-encapsulated hydrogels due to its fast gelation process, convenience, and ease of tuning porosity and mechanical strength.[27] Ionotropic crosslinking involves the interaction between the negatively charged carboxylate groups, especially in the G-block of alginate, and divalent or trivalent metal ions, such as Ca^{2+}, Sr^{2+}, Ba^{2+}, Cu^{2+}, Zn^{2+}, Mn^{2+}, Fe^{2+}, Cr^{3+}, and Fe^{3+}.[28] Calcium chloride is one of the most widely used gelling agents due to fast-crosslinking ability of Ca^{2+} with alginate. However, its application is limited by degelation under physiological conditions due to exchange of calcium ion with monovalent ions in surrounding media and the formation of heterogeneous gel crosslinks.[29] These processes result in weak mechanical stability, faster dissolution under physiological conditions, and heterogeneous porosity, which are suboptimal for long-term cell storage, growth, and proliferation in tissue engineering applications. The gelation and crosslinking of alginate using trivalent transition metal ions during the fabrication process can overcome the limitations of hydrogels constructed from divalent metal ions like calcium. Transition metals form strong coordinate covalent bonds by overlapping their partially filled d orbitals with the negatively charged carboxylate groups of alginates. The introduction of ferric ions as a gelling agent promotes the formation of such a coordinate covalent bond between iron and alginate, resulting in stronger and more stable hydrogels under physiological conditions.[30,31] To the best our knowledge, no previous studies have characterized and evaluated the biomedical properties of iron(III) cross-linked alginate–fibrillar chitin hydrogels and microcapsules.

In this study, we synthesized a composite hydrogel by blending alginate with chitin nanofibrils and crosslinking it using $CaCl_2$, $FeCl_3$, or a combination of both. Initially, we analyzed the rheological properties of the composite hydrogels. Next, we used electrospray techniques to create 3D microcapsules from the composite hydrogels. We then investigated the effects of these two different gelling ions on the mechanical strength and stability *in vitro* physiological conditions of these hydrogel constructs. The composite hydrogel microcapsules were utilized to encapsulate NIH3/T3 fibroblast cells, serving as a model to assess cell viability, growth, and metabolic activity of those encapsulated cells. While alginate-based microcapsules are well-established in tissue engineering, the incorporation of chitin fibrils and the use of trivalent ions present a unique advancement in the design of hydrogel scaffolds. This trivalent metal-ion (Fe^{3+}) crosslinking approach enhances the mechanical strength and structural stability of the microcapsules, while also providing an innovative platform for controlled drug release and cellular interactions. The use of chitin nanofibrils enhances mechanical strength and dimensional stability while also facilitating cell adhesion. Therefore, this study offers a versatile approach to the design of tailored microcapsules with potential applications ranging from tissue engineering to regenerative medicine.

Results and discussion

Characterization of hydrogel

A hydrogel is a soft material composed of a cross-linked network of hydrophilic polymer chains capable of absorbing and retaining water at levels up to hundreds or thousands of times their dry weight while maintaining structural integrity. This distinctive property enables a wide range of applications in drug delivery and tissue engineering. Characterizing physical, chemical, and mechanical properties of hydrogels is essential for assessing their suitability for biomedical uses. Thus, properties, such as viscoelasticity, surface morphology, and responses under physiological conditions were evaluated through rheological studies, SEM/EDX analysis, and mechanical stability tests.

Fig. 1 illustrates the fabrication process of alginate/chitin (60 : 40) hydrogel discs and microcapsules containing encapsulated cells. Electrospray technique was employed, using a flow rate of 3 mL h^{-1}, a voltage of 8 kV, and a nozzle-to-gelling bath distance of 40 mm.

Rheology of hydrogels. Hydrogels are considered non-Newtonian fluids with shear-thinning behavior.[32] As the shear rate increases, the viscosity of shear-thinning materials decreases,[33] while the viscosity of Newtonian fluids remains constant. This characteristic is crucial in fabrication of drug delivery microcapsules, 3D printing, and tissue engineering.[34,35] Strain sweep tests, also known as amplitude sweeps, are commonly employed in rheological characterization of hydrogels. These tests involve applying progressively increasing oscillatory strain at a constant frequency. The resulting data, expressed as storage modulus (G') and loss modulus (G'') as a function of strain, help identify the material's linear viscoelastic region (LVR), where the hydrogel exhibits stable mechanical behavior.

Fig. 2A illustrates the LVR of the hydrogels, characterized by a plateau at low shear strain, indicating that the storage moduli are unaffected by increasing shear strain. Fig. 2B and E display the average storage modulus and loss modulus of all three samples at LVR. All gel samples demonstrate a higher storage modulus than their respective loss modulus indicating they behave as semisolid gels with elastic properties. Notably, AF0 possesses substantially higher storage modulus compared to AC0, reflecting its enhanced elasticity and energy storage capacity against deformation. The comparison of loss moduli among three samples is illustrated in Fig. 2D where AF0 exhibits a markedly higher loss modulus than AC0. Calcium-gelled hydrogel demonstrates greater hydrophilicity than iron-gelled hydrogel, resulting in lower loss modulus. Fig. 2C and F show the crossover points of G' and G'' of AF0, and AC0, respectively. However, the crossover point of AFC is not shown here, all of these results indicate a marked transition in hydrogel behavior, shifting from elastic (*i.e.*, solid -like) to viscous (*i.e.*, liquid -like) characteristic.[36]

The primary objective of the strain sweep testing in this study was to identify the linear viscoelastic region (LVR) of the hydrogels, the region where the gel exhibits structural stability. The point at which the storage modulus begins to decline signals the onset of hydrogel disintegration or de-crosslinking. The broader LVR, along with higher storage and loss moduli and a gelation point at higher strain observed in ferric-ion-gelled hydrogels compared to calcium-ion-gelled hydrogels, suggests that ferric ions significantly enhance the elastic modulus more than divalent ions like calcium. Divalent ions form two-dimensional egg-box structures with alginate,[37] whereas trivalent ions, such as ferric ions, form more complex

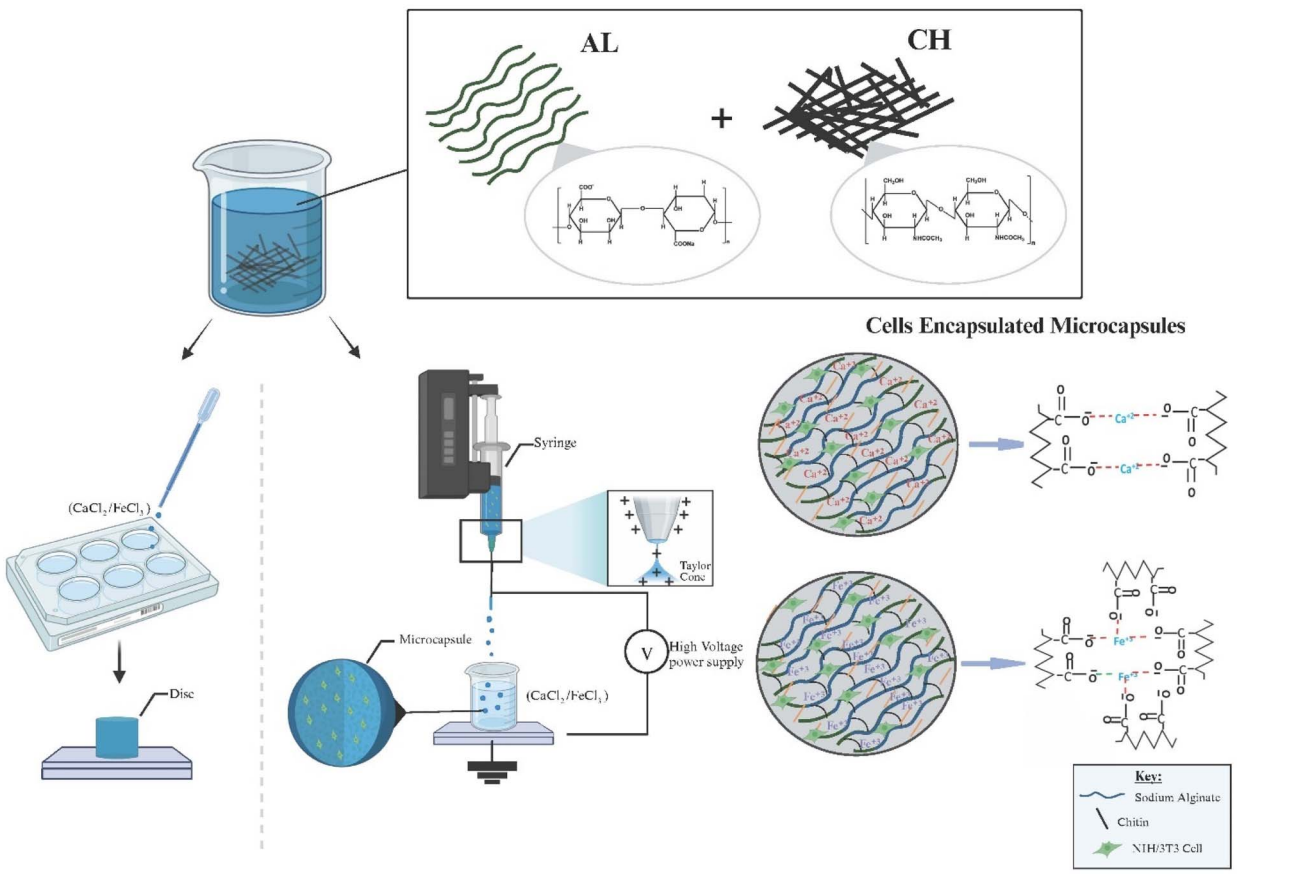

Fig. 1 Schematic illustration of the production of alginate/chitin discs and microcapsules and mode of interaction of alginate with Ca^{2+} or Fe^{3+} metal ions in gelling process along with their optical images.

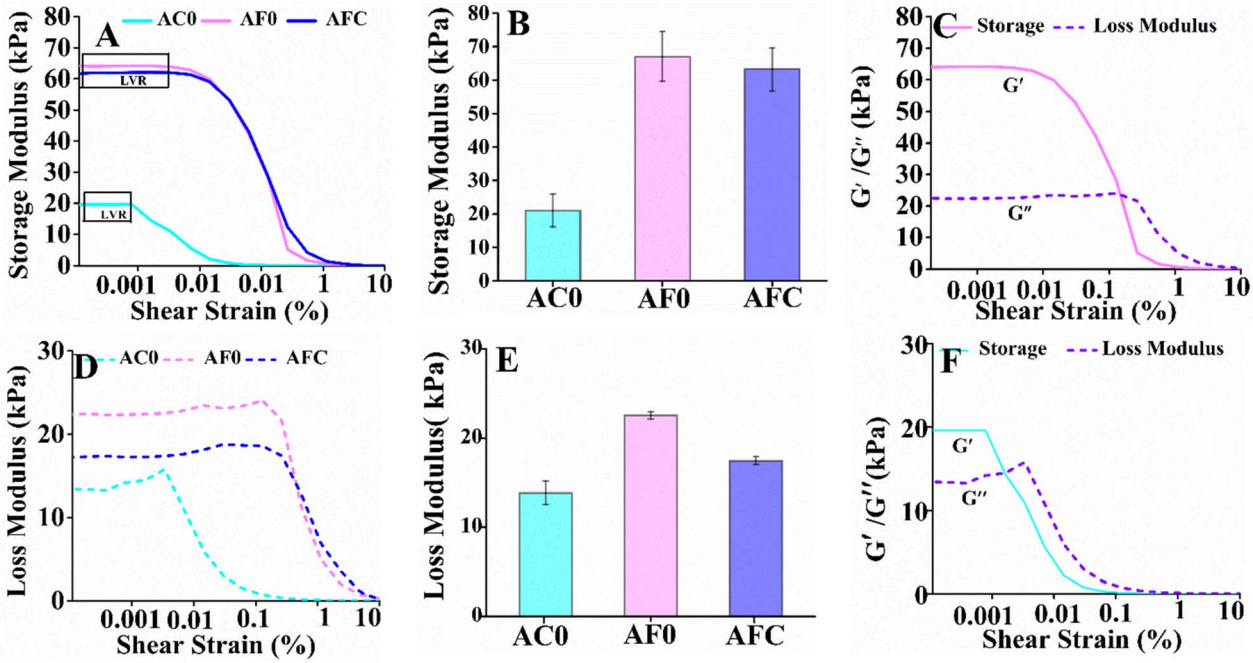

Fig. 2 Rheological analysis of hydrogels at 25 °C. (A and D) Changes in the storage and loss moduli of AC0, AF0 and AFC hydrogels as a function of shear strain. (B and E) Average storage and loss moduli of hydrogel samples measured from the plateau regions graphs of (A and D). (C and F) Plots indicating the crossover point of storage modulus (G') and loss modulus (G'') at different shear strain of AF0, and AC0 hydrogels, respectively. Moduli were measured for triplicate samples ($n = 3$).

three-dimensional structures. The ability of ferric ions to bind to both GG and GM blocks of alginate chains through coordinate covalent bonds results in a higher crosslinking density, creating a more compact network with improved mechanical properties, such as enhanced deformability under compressive and extensional stresses.[38] Consequently, Fe^{3+}-gelled hydrogels exhibit higher G' and G'' and a higher gelation point compared to calcium-gelled hydrogels, which have significantly lower G' and G'' values due to weaker interactions between alginate chains and calcium ions.

FTIR analysis. The FTIR spectra of the AC0, AF0, and AFC samples are shown in Fig. 3A. Analysis of these spectra reveals the presence of alginate functional groups and their interactions with Ca^{2+} and Fe^{3+}. A notable characteristic band observed in the range of 3000–3600 cm^{-1} corresponds to the stretching vibration of the O–H group in each sample. Compared to

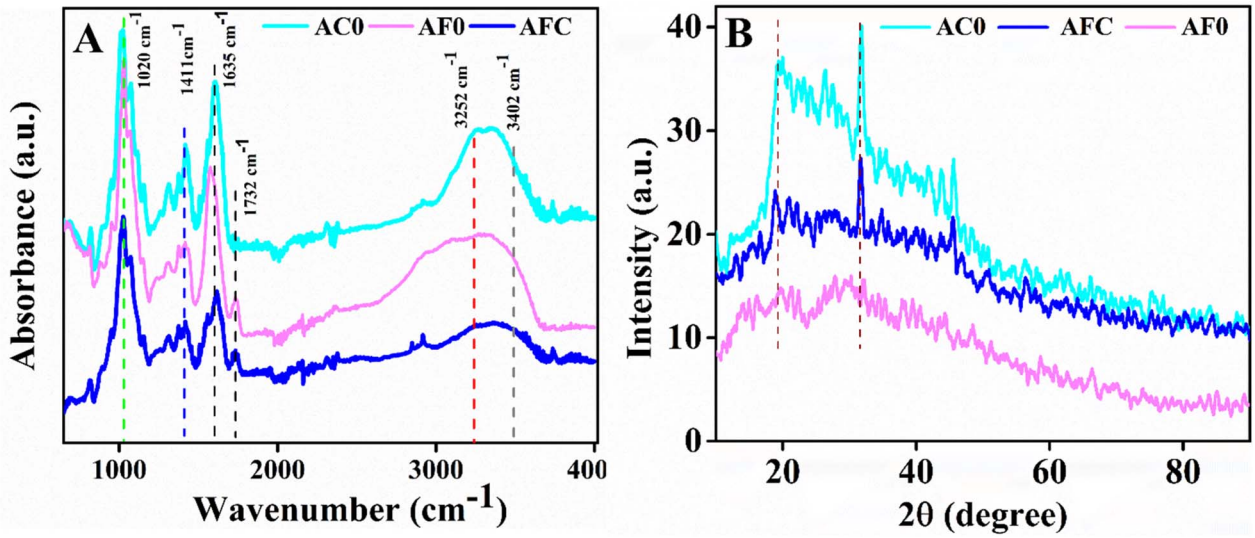

Fig. 3 Analysis of chemical structure and degree of crystallinity of hydrogel microcapsules. (A) ATR-FTR spectra of dried microcapsules and (B) XRD patterns of the microcapsules.

sodium alginate (data not shown), the O–H stretching vibrations in these samples are narrower. This narrowing can be attributed to interactions between hydroxyl and carboxylate groups of alginates with Ca^{2+} and Fe^{3+}, which form chelating structures, thereby reducing the number of hydrogen bonds among the OH groups. The narrower peak observed around 3300 cm^{-1} in AF0 samples indicates the higher number of interactions between ferric ion and hydroxyl groups of alginates, suggesting a greater susceptibility to these interactions compared to AC0 and AFC. The absorption bands with peaks at around 1576 and 1609 cm^{-1} correspond to the asymmetric stretching, while the absorption band with a peak around 1420 cm^{-1} corresponds to symmetric stretching vibrations of the carboxyl group ($-COO^-$) in alginate molecule.[18] In ferric and calcium gelled alginate, the asymmetric band was found shifted to lower wavenumbers at 1576 $cm^{-1}$and 1609 cm^{-1}, respectively, compared to sodium alginate at 1649 cm^{-1}.[39] These observations are consistent with previous studies, thereby suggesting the interaction of ferric and calcium ions with the carboxyl groups of alginate molecule.[18] Additionally, a new peak at appears at 1732 cm^{-1} in ferric gelled alginate, likely corresponding to vibration of the carboxyl group of alginate molecules. The notable difference in carboxyl group bands between Fe–alginate and calcium–alginate can be explained by stronger coordination ability of Fe^{3+} ions with alginate. Chitin is also confirmed in all three samples as evidenced by the characteristic peaks in the range of 1020–1030 cm^{-1} (C–O stretching) and additional peaks 1740, 1661, and 1560 cm^{-1}, corresponding to carboxyl, amide I, and amide II groups, respectively. These findings highlight the intricate interactions between the alginate chains and metal ions, which could have significant implications for the hydrogel properties and potential applications.

XRD characterization. XRD analysis was conducted to assess the purity, phase separation, and structural properties of the formulations. Fig. 3B presents the XRD pattern of AC0, AF0, and AFC powder samples. The peaks observed at $2\theta = 13°$ and 20° indicate the presence of sodium alginate and chitin, respectively in the hydrogel microcapsules.[40,41] In XRD patterns, the intensity of sodium alginate peak is notably higher in the AC0 sample compared to AFC samples while the AF0 sample lacks specific peak. This trend suggests a gradual decrease in the crystallinity of sodium alginate from AC0 to AFC, cumulating in a complete loss of crystallinity in the AF0 samples. In the AC0 sample, the molecular ordering of the alginate chains remains largely intact, as the binding of calcium ions does not fully

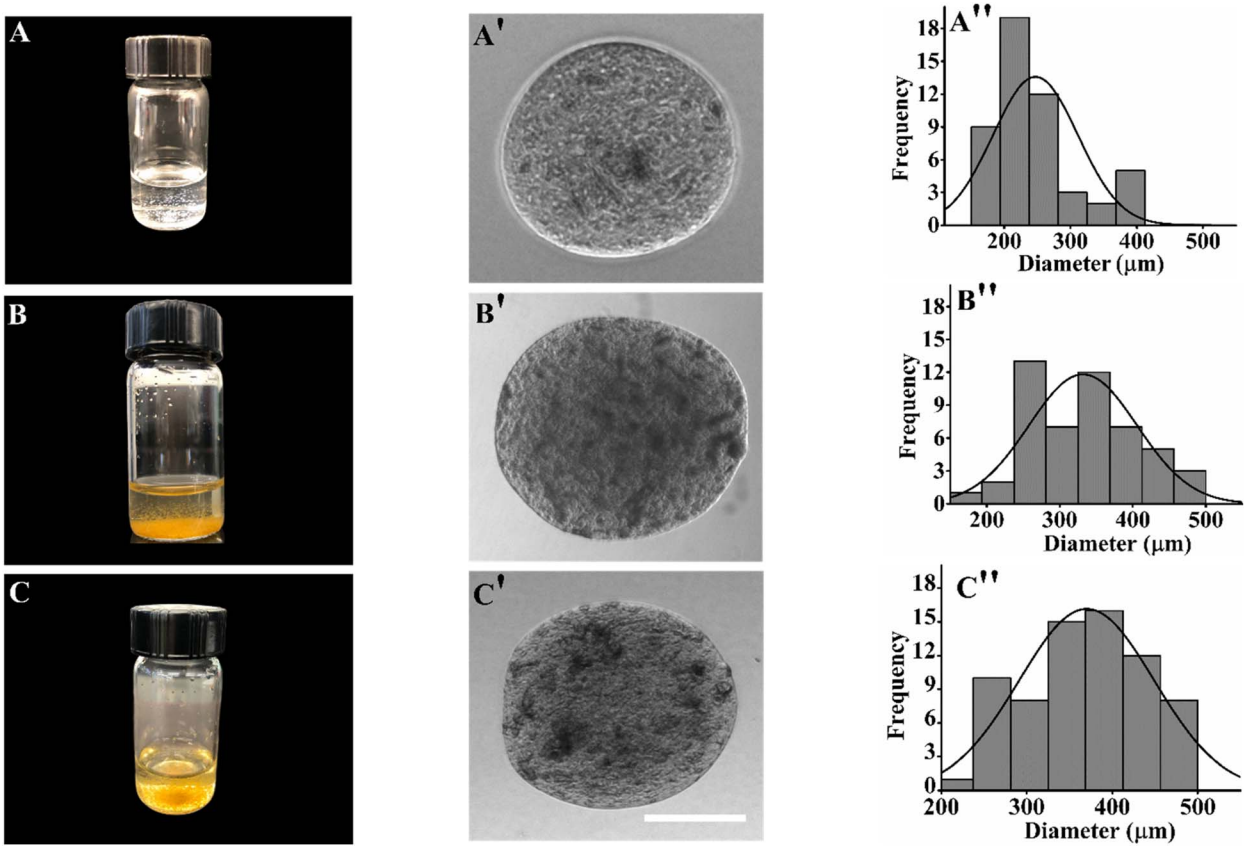

Fig. 4 Characterization of hydrogel microspheres. A, B, and C represent visual observation of as prepared microcapsules of AC0, AF0, and AFC. A′, B′, and C′ are representative optical microscopy images of as synthesized hydrogel microspheres. A″, B″, and C″ represent the histogram showing the size distribution of AC0, AF0, and AFC microcapsules, respectively. Average diameters of AC0, AF0, and ACF were 231 ± 51 μm, 393 ± 69 μm, and 361 ± 80 μm, respectively. Size of microcapsules were compared in DI water at 25 °C for $n = 50$ microcapsules. Scale bar = 200 μm.

disrupt the structure. This phenomenon may be attributed due to binding of one calcium ion with two chains of alginate while forming 2D model structure that leads to partial disruption of the molecular order yet retains some degree of crystallinity. Conversely, in the AF0 samples, one ferric ion binds with three alginate chains, resulting in the three-dimensional structure that significantly disrupts the molecular order, leading to complete loss of crystallinity in the alginate. This highlights the differing mechanism of crosslinking and their impact on the structural integrity of the alginate hydrogel.

Fabrication of microcapsules

Microcapsules were fabricated by extruding an alginate–chitin composite mixture using electrohydrodynamic atomization technique into beakers containing solutions of 150 mM calcium chloride, 150 mM ferric chloride, and mixture of calcium chloride/ferric chloride solutions (75 mM/75 mM). Fig. 4 displays photographic images of glass vials containing microcapsules, alongside individual optical microscopic images and their size distribution profiles. The visual observation indicate that all three gelling baths produced spherical microcapsules from the chitin-incorporated alginate solutions. The size distribution of the microcapsules ($n = 50$) is quantitatively represented in a frequency distribution histogram, revealing average sizes of 231 μm for AC0, 393 μm for AF0, and 363 μm for AFC. The narrow size distribution and smaller size of AC0 microcapsules, in comparison to AF0 and AFC, can be attributed to purely ionic interactions and reduced gelation time between calcium and alginate chains. In contrast, the larger size of AF0 and AFC microcapsules is a result of slower gelation process due to coordinate covalent interactions between ferric ions and alginate chains. It has been reported that the mechanical and chemical stability of microcapsules depend largely on their sphericity, with spherical microcapsules exhibiting higher mechanical strength compared to non-spherical beads.[42] The use of electrospray techniques for fabrication of alginate microcapsules have been reported in numerous studies.[43–45] To our knowledge, this is the first report detailing the successful fabrication and characterization of stable, spherical, and reproducible Fe^{3+} and Fe^{3+}/Ca^{2+}-gelled alginate microcapsules incorporated with chitin fibrils, using optimized parameters, such as voltage, solution concentration, and flow rate. This advancement holds significant promise for applications in drug delivery, cell culture, and biomedicine, where microcapsule stability plays a crucial role.

SEM analysis. The external morphology and the elemental percentage composition of freeze-dried AC0, AF0, and AFC microcapsules were analyzed using a Scanning Electron Microscope (SEM) and Energy Dispersive X-ray (EDX). As illustrated in Fig. 5, the SEM image of AC0 reveals a compact, less porous morphology compared to AF0 and AFC microcapsules. The binding of divalent cations, such as Ca^{2+}, Ba^{2+}, and Zn^{2+} with alginate occurs in a planar two-dimensional manner, leading to relatively rigid surfaces with lower porosity.[28] In contrast, the SEM image of AF0 microcapsules exhibit a spongy, rough, and highly porous surface morphology. This increased porosity is attributed to the ability of ferric ions to form coordinate covalent bonds with carboxylate groups of multiple alginate chains, resulting in a three-dimensional network structure. The rough surfaces of these microcapsules facilitate enhanced protein adsorption, and the greater porosity promotes better exchange of

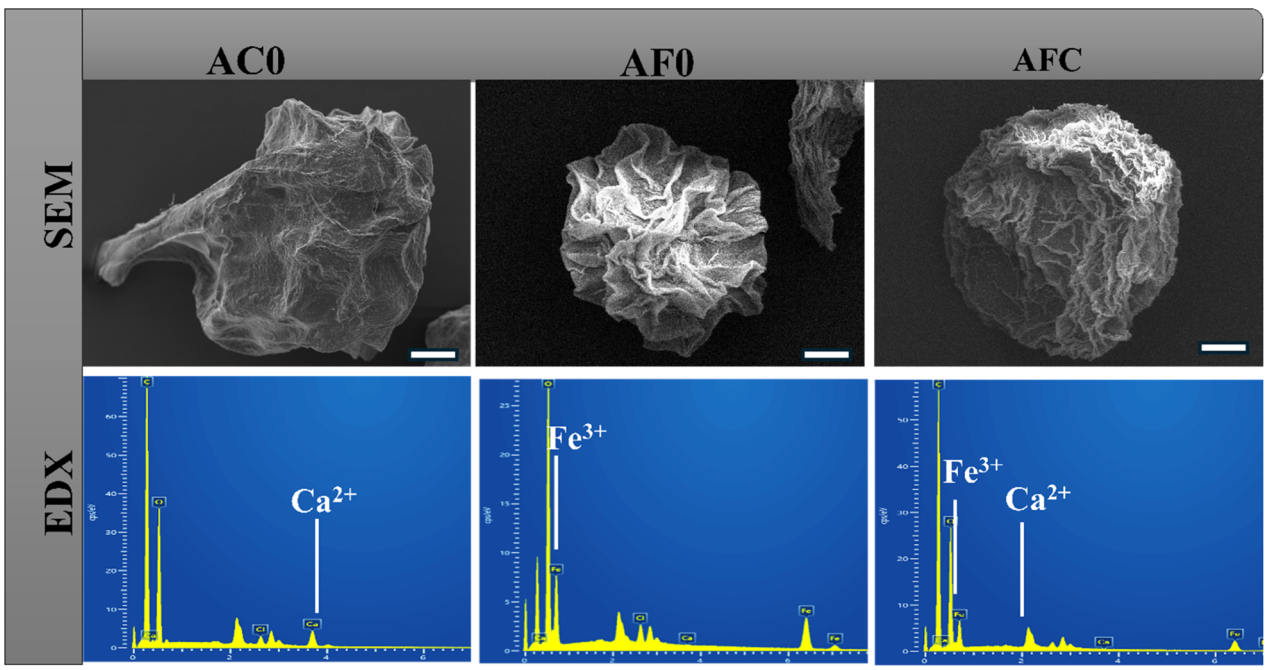

Fig. 5 Characterization of surface morphology and determination of elemental composition of lyophilized microcapsules. SEM micrograph of lyophilized AC0, AF0 and AFC microcapsules at the top panel and EDX analysis of the respective microcapsules depicting elemental percentage composition at bottom panel. Scale bar = 50 μm.

nutrients and metabolites critical for cell growth and proliferation. In EDX spectrum of the samples, the prominent peaks at 3.7 keV and 6.4 keV is the clear indication of the presence of calcium and ferric ions in AC0 and AF0 samples, respectively. Therefore, the appearance of these peaks confirms a successful incorporation of calcium and ferric ions in corresponding hydrogel during gelation of sodium alginate.

Mechanical strength and stability study. The mechanical properties of AC0, AF0, and AFC microcapsules were assessed through compressive stress–strain tests with the resulting force–displacement curves illustrated in Fig. 6A. The analysis revealed that Ca^{2+}-gelled microcapsules required higher force for the same displacement compared to those gelled with ferric ions or combination of calcium and ferric ions. Young's modulus was calculated from these curves, and the results are presented in Fig. 6B. The data indicate that the microcapsules gelled with calcium ions exhibited a higher Young's modulus than those gelled with ferric ions or the combined ions. The increased Young's modulus observed in calcium-gelled microcapsules can be attributed to their more rigid structure arising from rapid gelation due to purely electrostatic interactions between alginate and calcium ions. Conversely, the slow gelation process due to the formation of coordinate covalent bonds between ferric ions and alginate leads to a hydrogel that requires a slightly less force to achieve the same displacement.

The stability of microcapsules in various media, especially water, complete media, and PBS was evaluated by submerging them into these media and incubating at 37 °C in a humidified condition with 5% CO_2. As shown in Fig. 6D, no substantial size changes were observed for AF0 and AFC microcapsules in DI water and complete media. In PBS, these microcapsules experienced noticeable size changes. However, the size change is particularly notable when comparing the AC0 microcapsules. The size of the AC0 microcapsules was nearly doubled in PBS as

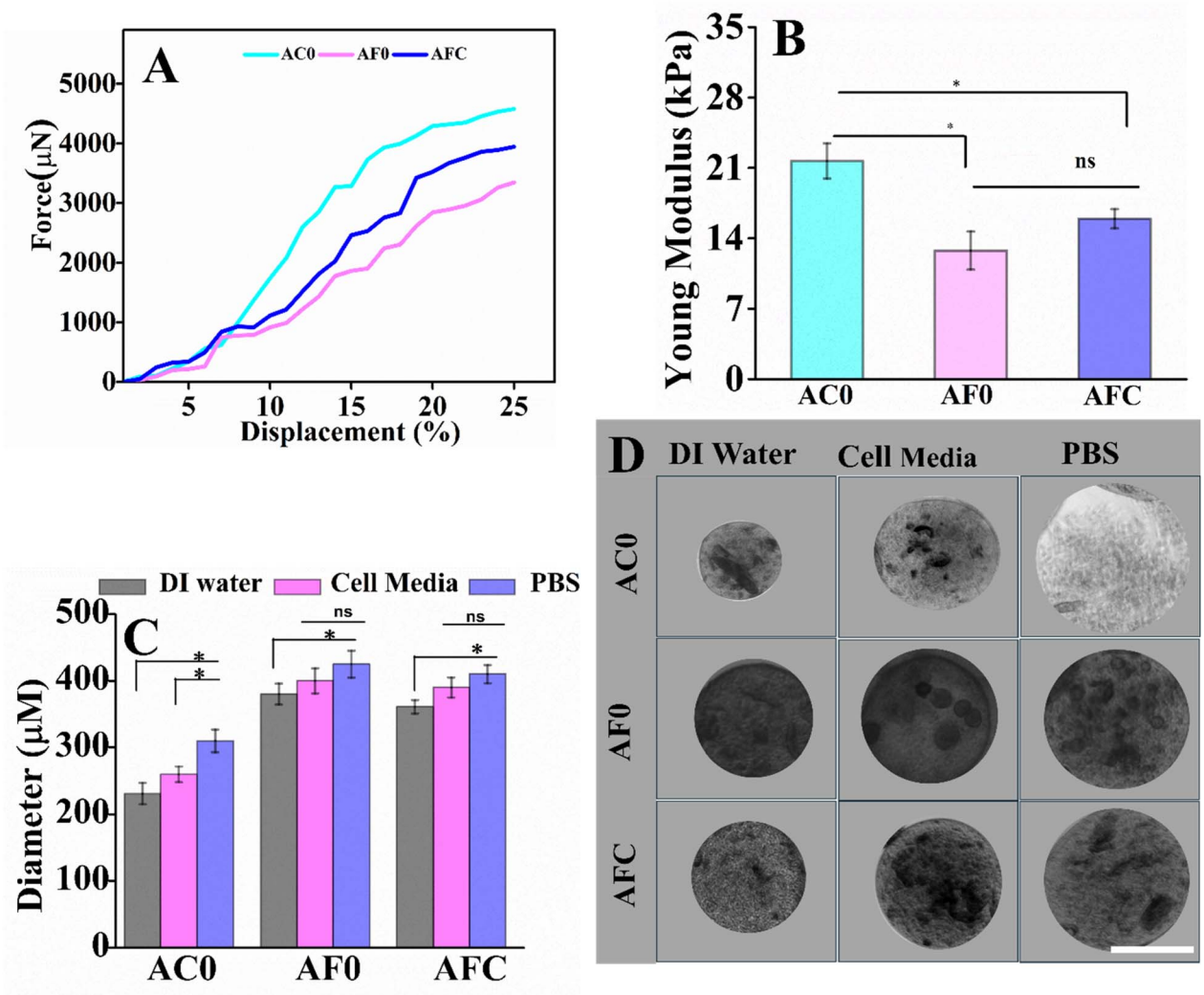

Fig. 6 Analysis of mechanical properties and the stability of microcapsules incubated in different media for 24 h at 25 °C. (A) Representative force displacement curves of microcapsules incubated in DI water. (B) Young's modulus of the microcapsules ($n = 5$). (C) The size distribution of AC0, AF0, AFC microcapsules submersed in Di water, cell media, and PBS. (D) Microscopic images of microcapsules in the different media. Scale bar = 200 μm. Statistical analysis was performed using the one-way ANOVA with Tukey's post hoc method, where * indicates statistically significant at $p < 0.05$.

compared to that in water. The substantial increase in microcapsule size in complete media and PBS is likely due to losing the tight junction among chains caused by the exchange of gelling ions (*i.e.*, Ca^{2+} and Fe^{3+}) with monovalent ions (*i.e.*, Na^{+} and K^{+}) from the media and buffer during the incubation period. The photographic images in Fig. 6D reveal that all three types of microcapsules remained swollen while maintaining their spherical integrity.

The stability of the cell-laden matrix in aqueous system is crucial for regulating cell behavior, including survival, development, migration, proliferation, shape, and functions. Our observations demonstrate that AF0 microcapsules retained their structural integrity even after during multiple washes in PBS. In contrast, AC0 microcapsules exhibited structural degradation, likely due to exchange of calcium ions within the gel with monovalent ions in PBS. The coordination chemistry between alginate and metal cations plays a critical role in determining stability of microcapsules in PBS. Studies indicates that interaction between uronate units of alginate and alkaline earth metal ions is primarily electrostatic, while transition metal ions form coordinate covalent coordination complexes.[46,47] As a result, the interactions between alginate and ferric ions are stronger than those with calcium ions, and this explains the greater stability of AF0 and AFC microcapsules in PBS compared to AC0 microcapsules.

Additionally, the binding strength of cations is influenced by their ionic radius and charge density. Calcium ions have an ionic radius of 0.99 Å and a charge density of 0.49 $eÅ^{-3}$ while ferric ions have a smaller ionic radius of 0.55 Å and a much higher charge density of 4.30 $eÅ^{-3}$.[48] The smaller ionic radius and higher charge density of ferric ions create stronger bonds with carboxylate ions, leading to superior physicochemical properties in Fe^{3+}-gelled microcapsules. The superior mechanical properties of ferric ion-gelled alginate microcapsules are further corroborated by a drastic change in appearance of cell-encapsulated microcapsules after multiple wash with PBS (see Section cell incapsulation and Fig. 10). Multiple washes with PBS during rhodamine/DAPI staining showed that Ca^{2+}-gelled microcapsules underwent degelling while Fe^{3+}-gelled microcapsules maintained their structural integrity, as indicated by the fluorescence images.

Cell encapsulation, cell toxicity, and proliferation studies

The optical images of NIH/3T3 cell-encapsulated microcapsules are presented in Fig. 7. The microcapsules exhibited spherical morphology with sizes ranging from 450–550 μm for AC0, 600–700 μm for AF0, and 550–650 μm for AFC. Notably, Fe^{3+}-gelled microspheres were slightly larger than those gelled with calcium or a combination of both ions. Cell distribution within the microspheres was uniform, with minimal cell presence on

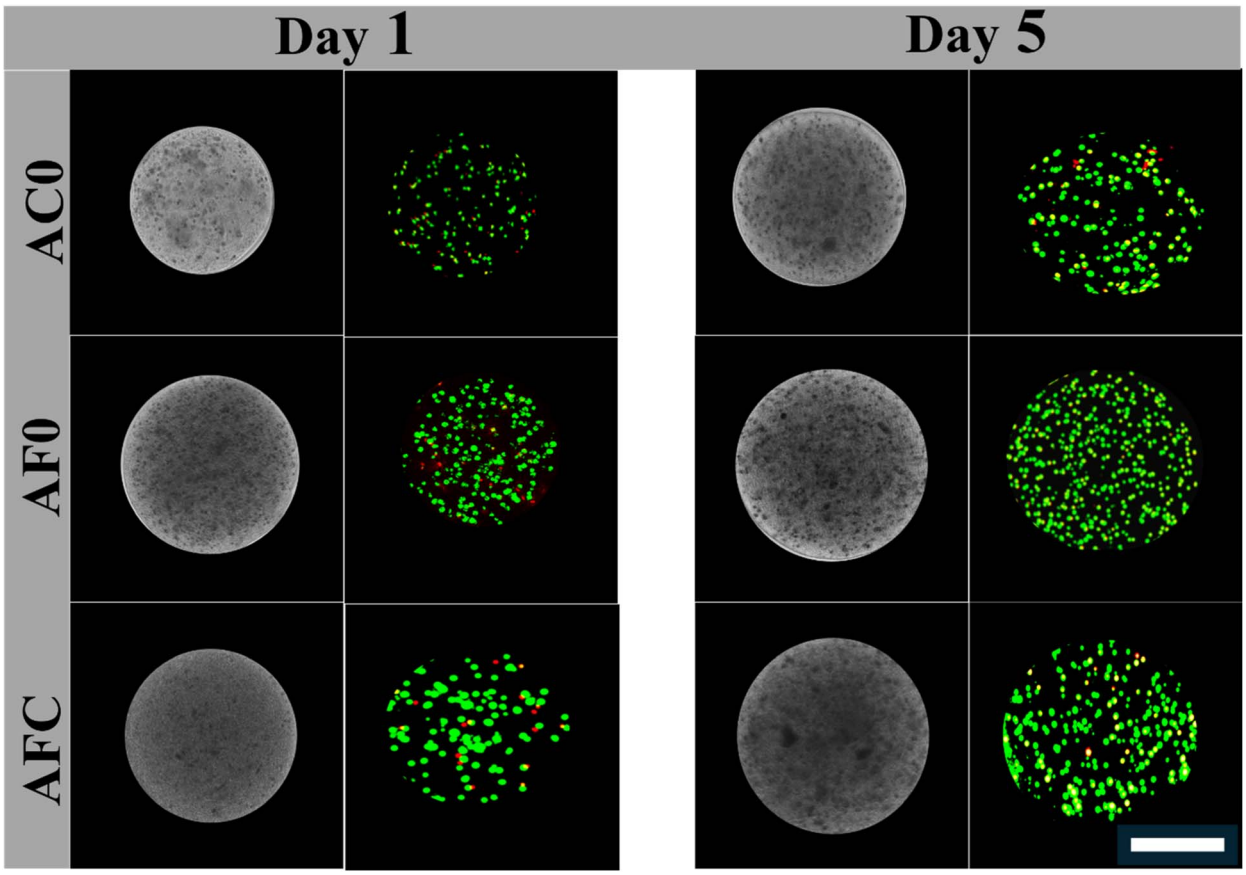

Fig. 7 *In vitro* performances of microcapsules and cell viability study. The bright field image and fluorescence images of cell-encapsulated microspheres representing live (stained green) and dead (stained red) NIH/3T3 fibroblast. Cells were stained by AOPI scale bar = 200 μm.

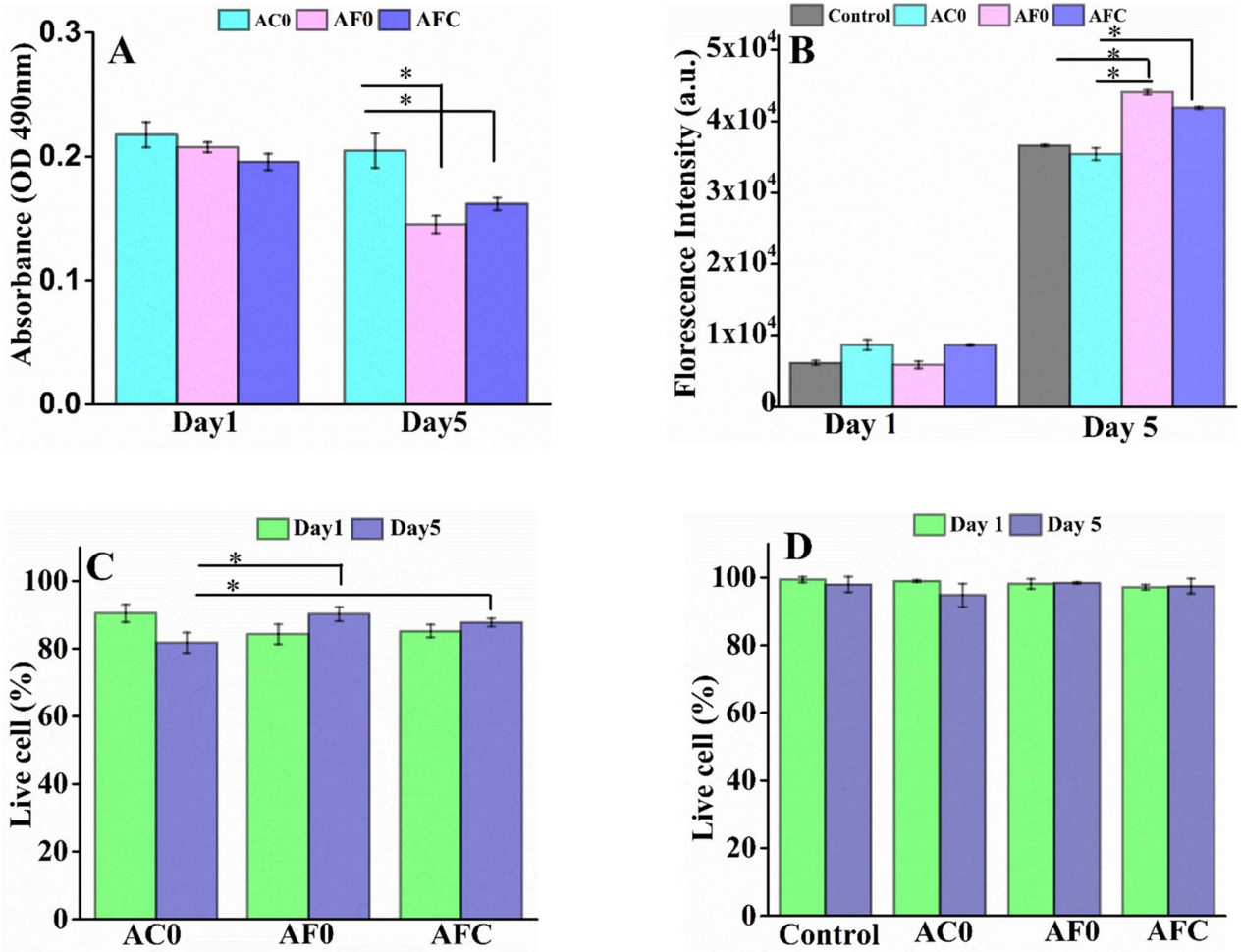

Fig. 8 *In vitro* analysis of microcapsules with NIH/3T3 fibroblasts and performance on cell viability and cell attachments studied by LDH assay and live-dead staining. (A) The cytocompatibility of cell-encapsulated microcapsules by measuring the absorbance at 490 nm to quantify LDH released at day 1 and 5 ($n = 3$). (B) The histogram of fluorescence intensity for metabolic activity of cells encapsulated in the microcapsules as measured by AlmarBlue assay at day 1 and 5. (C) Histogram showing the percentage of live cells in fluorescence image of cell-encapsulated microcapsules prepared in different gelling baths ($n = 5$). (D) The histogram showing the percentage of live cells cultured with extracted media from the incubated microcapsules at day 1 and 5.

the surfaces. This study represents the first successful fabrication of cell-encapsulated alginate–chitin microspheres using the electrospray technique in ferric ion and ferric/calcium ion gelling baths. The additional electrospray parameters, such as applied voltage, needle tip-to-gelling bath distance, needle gauge, and flow rate were optimized during cell encapsulation according to prior publications.[49]

To evaluate cell viability and proliferation within the microcapsules, we conducted LDH and AlamarBlue assays on the media collected from the encapsulated cells at days 1 and 5. Fig. 8A illustrates the LDH assay results, expressed in absorbance, from the cell media collected on those days. The data indicate that AF0 and AFC microcapsules exhibited low absorbance on days 5, suggesting minimal toxicity and high cell survival rates compared to day 1 and AC0. Correspondingly, the AlamarBlue assay results in Fig. 8B reveal a marked increase in cell proliferation, with fold increase of 2.6, 3.6, and 3.1 from day 1 to 5, for AC0, AF0, and AFC microcapsules, respectively. Notably, AF0 microcapsules demonstrated substantially higher cell proliferation than both AC0 and AFC, likely due to their softer, spongy structure, and enhanced porosity, which facilitate a better nutrient and metabolite exchange. Fig. 8C depicts the percentage of live cells within the microcapsules at days 1 and 5, with live cells exceeding 80%, across all samples until day 5. Importantly, AF0 microcapsules maintained a higher percentage of live cells compared to AC0 and AFC. The histogram in Fig. 8D shows the percentage of live cells on day 1 and 5 when cells cultured in extracted media from submerged microcapsules, with corresponding fluorescence images presented in Fig. 9. Live cells remained above 95% in all three samples, underscoring the biocompatibility of the microcapsules for cell growth and proliferation.

The AF0 hydrogel demonstrates higher cell viability and proliferation rates compared to calcium alginate gels. This observation underscores the importance of microcapsules in optimizing the performance of hydrogel for applications in

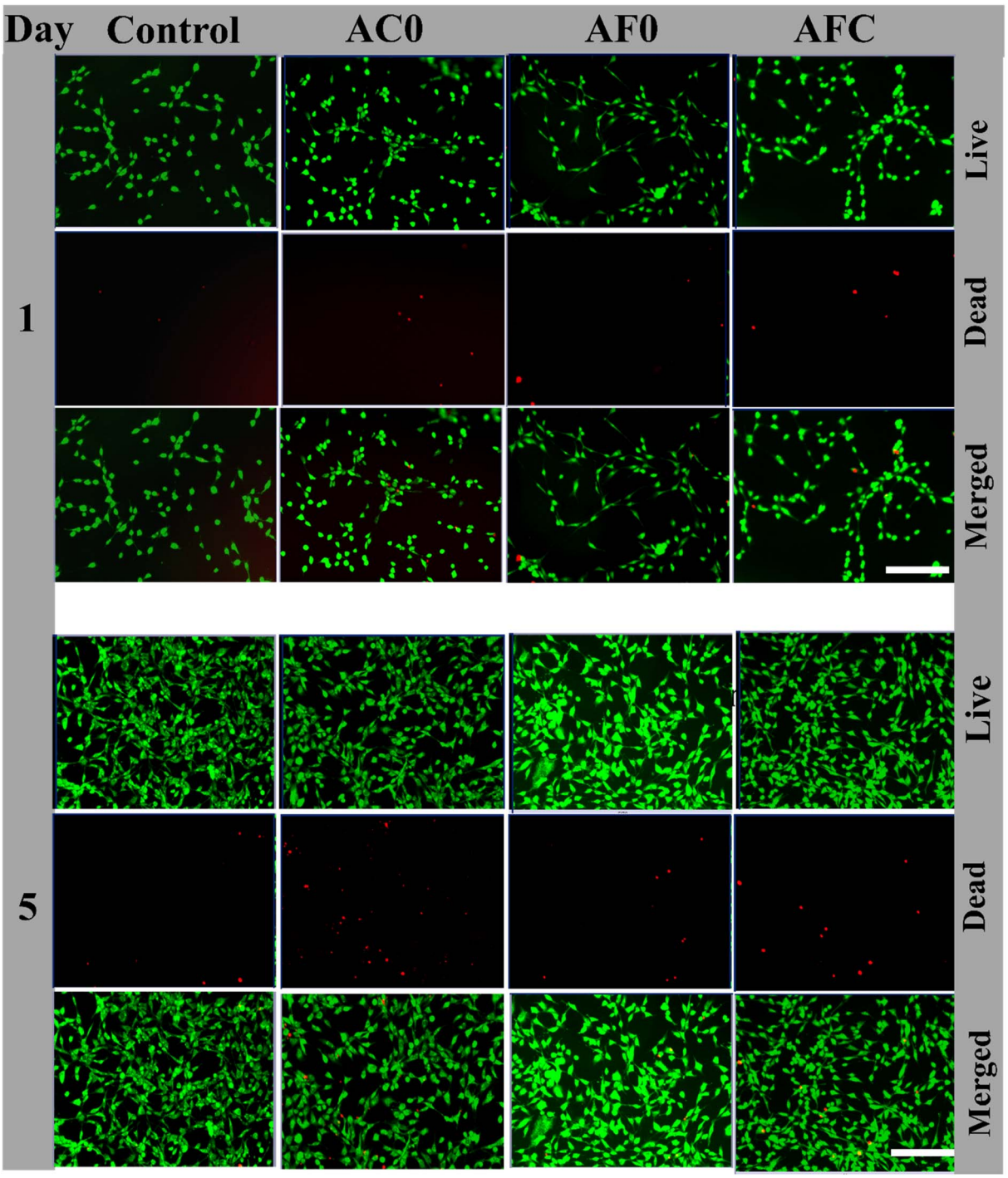

Fig. 9 *In vitro* performance and cell viability study in extracted media of microcapsules. The fluorescence image of NIH/3T3 cells cultured in extracted media on day 1 and day 5 representing live (stained green) and dead (stained red). Cells were stained using AOPI. Scale bar = 200 μm.

tissue engineering and regenerative medicine. This enhancement of cell viability, growth, and proliferation in ferric-gelled microcapsules can be attributed to protein adsorption, particularly vitronectin, a glycoprotein crucial for cell adhesion, migration, and proliferation.[50,51] Fe^{3+}-gelled hydrogels are considered to more hydrophobic leading to increased protein adsorption, while hydrophilic nature of calcium alginate results in reduced protein contact. Consequently, as reported in previous studies, Fe^{3+}-gelled alginate hydrogels promote better cell proliferation compared to Ca^{2+}-gelled alginate hydrogels due to their enhanced protein adsorption.[51]

Cell morphology

After confirming sufficient cell growth within the cell-encapsulated microcapsules, we focused on evaluating cell morphology in both a 2D surface environment and a 3D

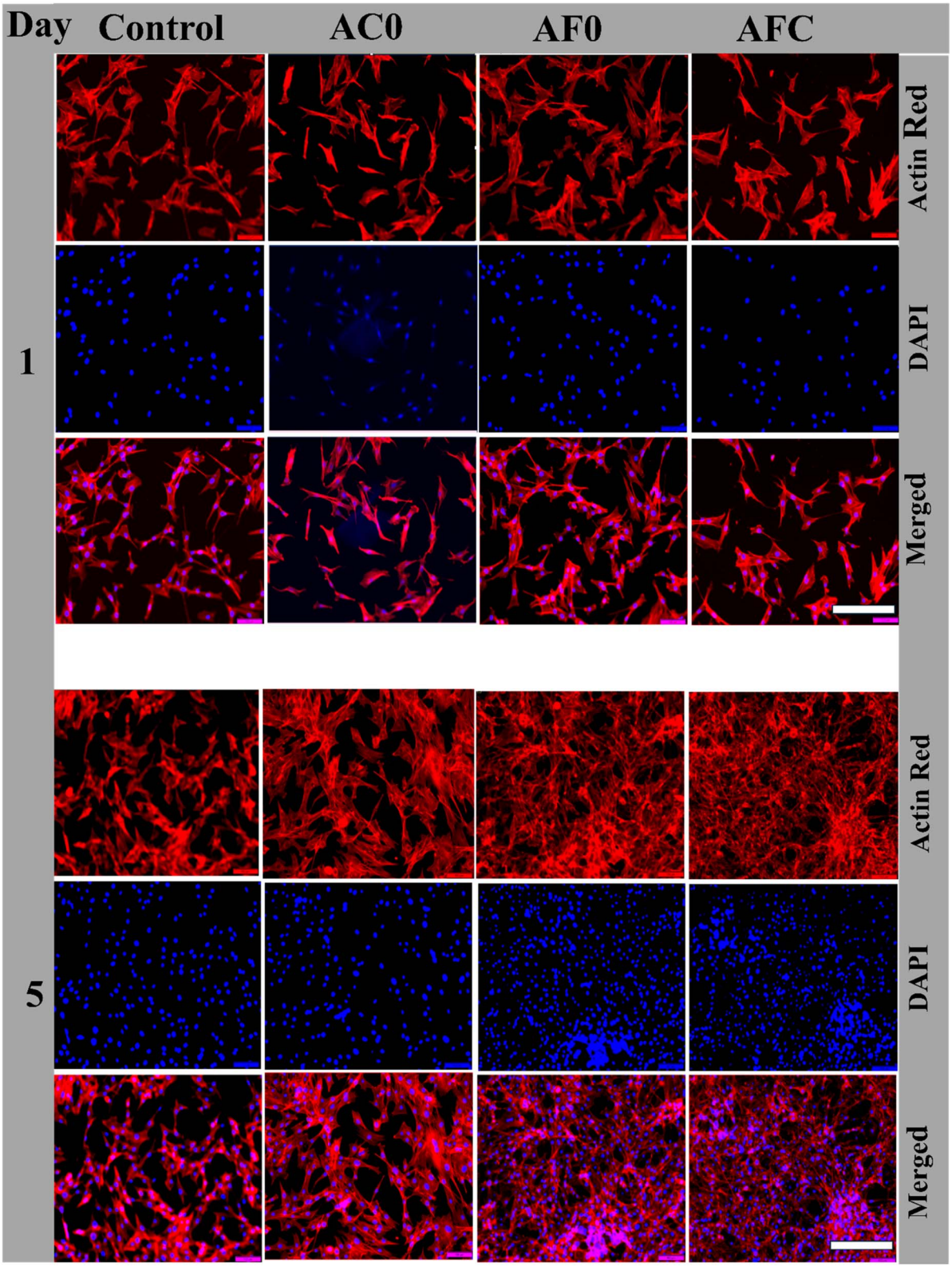

Fig. 10 Study of NIH/3T3 fibroblasts cell proliferation and morphology cultured on extracted media of AC0, AF0, AFC microcapsules, and control media. Fluorescence microscopy images of the NIH/3T3 fibroblasts cultured in the extracted media after day 1 and day 5. The cytoskeletons were stained by rhodamine-phalloidin (red) and counter-stained with DAPI (blue) for the nuclei. Scale bar = 100 μm.

structure. Fluorescence microscopy images of the cells grown in the extracted media from AC0, AF0, and AFC microcapsules on days 1 and 5 are presented in Fig. 10. The fluorescence images display extended cytoskeletons, dendritic structures, and polygonal shapes, all indicative of healthy cell morphology. By day 5, increased cellular mass density suggests robust growth and proliferation, confirming the biocompatibility of all microcapsule types. The cells were uniformly distributed and well spread on the surface. Notably, the cell body in 2D seems flattened and elongated extensively spread throughout the surfaces, exhibiting extensive outgrowth of pseudopodia. Further, the cells' adhesive nature and spindle-like structure on cell morphology were observed in the control and AC0 samples. However, in the AF0 and AFC samples, the cellular mass density is high resulting in excessive cell growth, suggesting that the extracts provide a strong biomimetic surface to coordinate cell growth, proliferation, and regeneration.

Further, the fluorescence microscopy images of encapsulated NIH/3T3 cells within the 3D microcapsule after 5 days of culture are depicted in Fig. 11. Within the microcapsules, cells retained round or slightly elongated shapes due to spatial confinement, which restricted cell spreading and resulted in a more compact morphology. The compact morphology of cells in AC0 microcapsules was less distinct due to gradual degelation in PBS during washing. In contrast, AF0 and AFC microcapsules exhibited compact cell morphology, clear cytoskeletal structures, and well-defined nuclear staining, indicating active cell proliferation. The cells were well-proliferated and distributed relatively similar to the cell cultures in 2D structures. The proliferation of cells was not affected in the microcapsules. Interestingly, the porous structure of the alginate/chitin hydrogel microstructure exhibited a favorable environment for cell growth and spreading. The cells were uniformly distributed. The staining of nuclei (blue color) and filamentous cytoskeleton (red color) were observed in

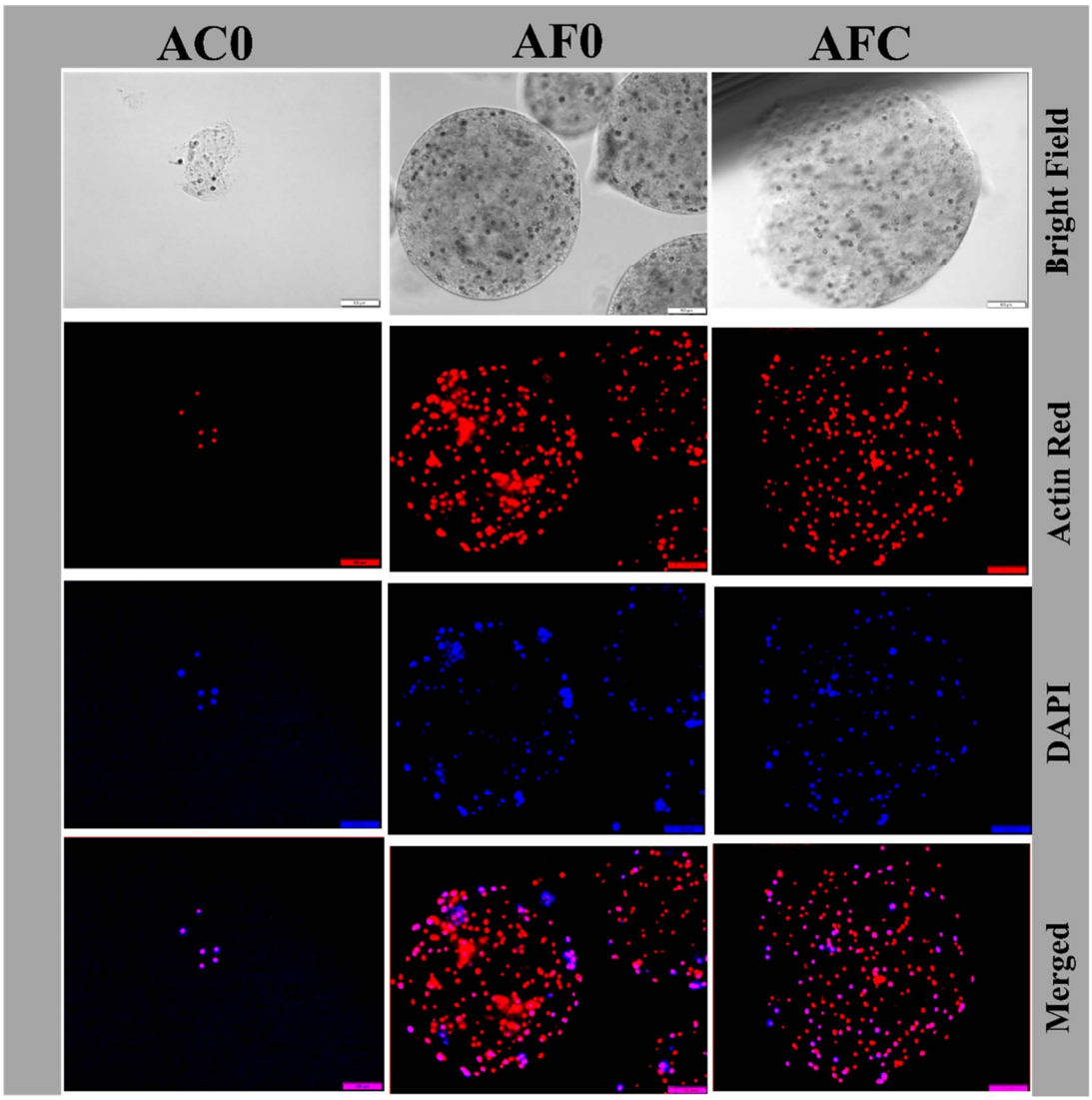

Fig. 11 Study of NIH/3T3 fibroblast cell morphology and proliferation within AC0, AF0, and AFC microcapsules, cultured for 5 days. Bright-field image (top panel) of cell-encapsulated microcapsules followed by the fluorescence microscopy image as rhodamine-phalloidin (red) for cytoskeleton, DAPI (blue) for nuclei scale bar = 100 μm.

the 3D structured hydrogel microcapsules enhancing the cell body to be able to sense and respond to the signals from surrounding surface topography for cell proliferation and differentiation.[52] According to Semenyuk *et al.* and Tatum *et al.*, the spongy microcapsule hydrogel has cationic and anionic charges which influence protein interaction and biomolecules diffusion, thereby inducing biological activity.[53,54] Cells grown in fibrous hydrogels benefit from proper attachment sites, concentration gradients for bidirectional flow of nutrients, oxygen, and metabolites, adequate cell communication, and tissue-like stiffness; all of which enhance the mimicry of the *in vivo* microenvironment. Consequently, cell morphology and molecular mechanisms are preserved in cells grown in microcapsules, as illustrated in Fig. 11. From a morphological perspective, AF0 microcapsules appeared to support healthier and more proliferative cells compared to AC0 microcapsules, highlighting the beneficial effects of the ferric ion environment on cell viability and morphology. This finding aligns with previous studies that have demonstrated positive effects of ferric ions on cellular behaviors. Ferric ions have been known to participate in various biological processes, including the regulation of cellular growth, repair and differentiation.[55] For example, iron plays a crucial role in cellular metabolism, particularly in oxygen transport and energy production, which could explain the observed improvement in cell health and morphology in the Fe^{3+}-gelled microcapsules.[56] In contrast, calcium ions, though essential for cell signaling, may not provide the same level of support for proliferation in this context, potentially due to differences in the biochemical pathways they regulate.

Additionally, the structural integrity of the microcapsules could contribute to the observed differences. Ferric ions may influence the mechanical properties of the gel matrix, creating a more supportive environment for cell attachment and growth. On the other hand, Ca^{2+}-gelled microcapsules may form a less optimal structural network, potentially limiting cell expansion and attachment, which could explain the reduced cell proliferation observed in this condition.

Cell migration

To investigate the effects of calcium and ferric ions on cell migration and proliferation, we conducted a scratch assay on the monolayer of NIH/3T3 cells cultured in media extracted from different microcapsules and a control cultured medium in 24-well plates. Fig. 12 shows the optical images of the scratched-wound healing process. The results demonstrate that the scratch was progressively filled due to cell migration and proliferation of cells towards the scratched area. The corresponding histogram represents the relationship between cell-free area and time. The media extracted from ferric ion crosslinked microcapsules (AF0 and AFC) demonstrates a gap closure percentage of 80 and 75%, respectively, compared to 65% for the calcium ion-crosslinked AC0 microcapsules after 18 hours. This illustrates that a rapid migration and proliferation of NIH/3T3 fibroblast cells occur due to improved adsorption of serum proteins like vitronectin and fibronectin in a ferric ion-enriched environment.[56] This aligns with existing literature indicating that ferric ions enhance serum protein adsorption, thereby improving fibroblast cell adhesion *via* their binding receptors, αv and β1 integrins.[51] In contrast, the lower protein adsorption observed in Ca^{2+}-gelled microcapsules resulted in a slower migration and proliferation as illustrated in Fig. 12. Hence, increased protein adsorption facilitated by media from Fe^{3+}-gelled microcapsules supports enhanced cellular adhesion, spreading, and proliferation.

This methodology relies on the principle that when a scratch is made on the confluent cell monolayer, cells at the edge of the gap migrate to close the scratch, thereby re-establishing new cell–cell contacts. By observing the collective migration of cells in a controlled *in vitro* environment, we can simulate key mechanisms involved in cell migration and proliferation, which presents the promising potential of the hydrogel for applications in skin tissue engineering and other biomedical fields. The study of cell migration and proliferation is crucial for various physiological processes, such as wound healing, embryonic development, and angiogenesis. This research aims to mimic aspects of *in vivo* cell migration. Recent findings suggest that the ferric ion-enriched environment supports cell proliferation due to the adsorption of serum proteins, such as vitronectin and fibronectin, resulting in improved fibroblast proliferation. The coordinate covalent complex formed between alginate and ferric ions contributes to the mechanical strength and porosity of the microcapsules, which are advantageous for a long-term cell culture. In contrast, the purely electrostatic interactions in calcium alginate lead to a rigid structure with lower porosity, impeding adequate nutrient exchange and consequently slowing cell growth and proliferation. Additionally, chitin-integrated alginate composites enhance cell interactions due to their low toxicity, hydrophilicity, mucoadhesive properties, and hemostatic abilities, all of which support wound healing.[57] These composite materials also play a crucial role in stabilizing reactive oxygen and nitrogen species generated during cellular metabolism, thereby reducing the oxidative and nitrosative stress, which are key contributors to cell damage and death.[58] Overall, our findings suggest that Fe^{3+}-gelled hydrogel microcapsules offer a promising alternative to Ca^{2+}-crosslinked hydrogel microcapsules for enhancing cell adhesion, growth, proliferation, and migration. Further, cellular microencapsulation provides a strategy for immobilizing cells within biomaterials, addressing immunogenicity by blocking larger molecules while allowing the diffusion of smaller molecules such as oxygen and nutrients. This encapsulation not only promotes immunoisolation but also influences intracellular processes such as cell phenotype, cytoskeleton organization, proliferation, and migration. This finding is consistence with our previous research demonstrating the efficacy of cell encapsulation in alginate–chitin composite core–shell microcapsules.[49] Thus, it can be concluded that Fe^{3+}-gelled hydrogel microcapsules encapsulated with cells could serve as a highly efficient system for regenerative medicine, cell delivery, drug delivery, wound healing, and tissue engineering applications.

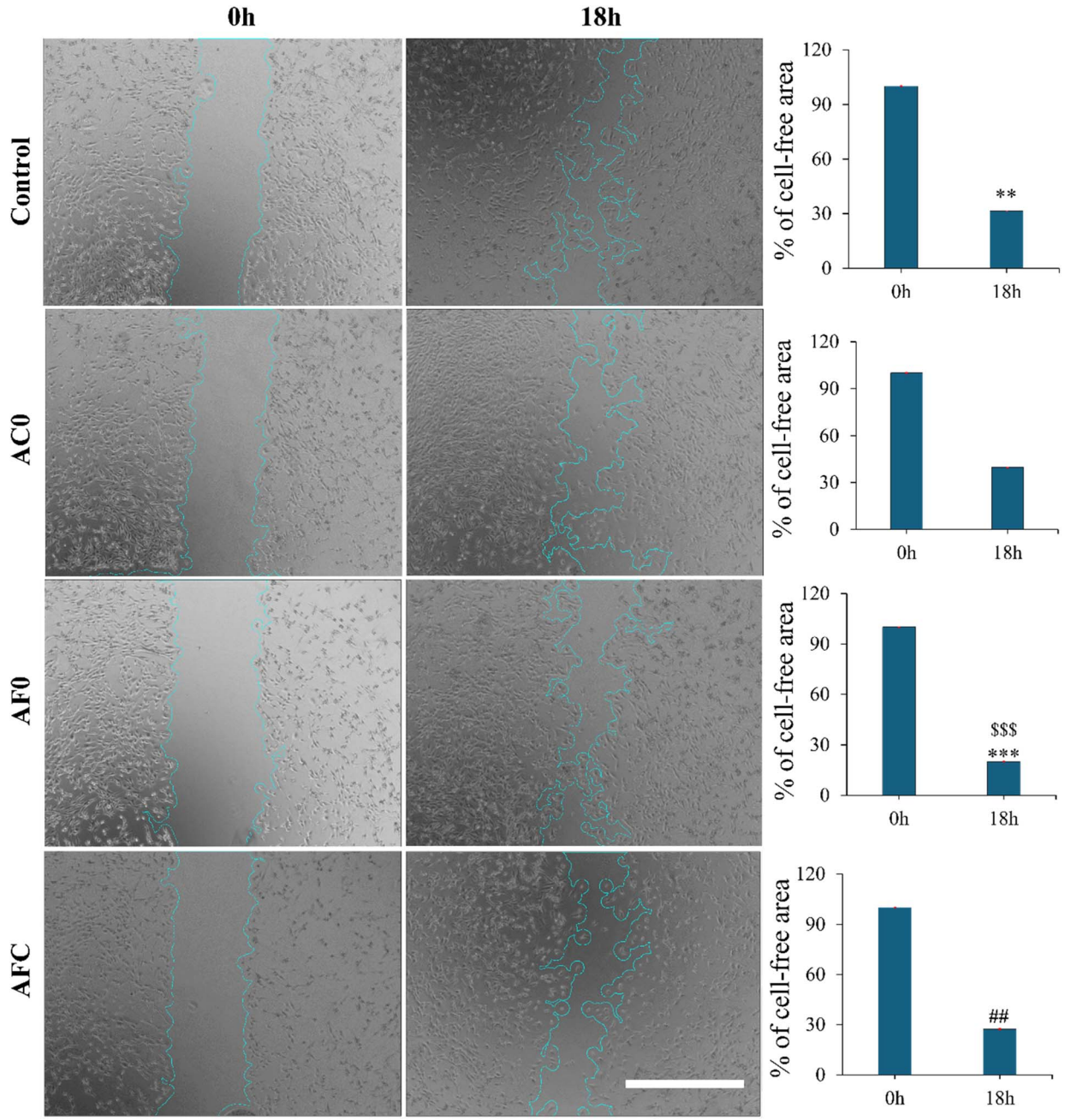

Fig. 12 Representative images and corresponding quantitative analysis from *in vitro* scratch-wound healing assay demonstrating that NIH/3T3 cell migration into the cell-free region as marked with blue lines cultured in media extracts of different microcapsules. The migratory ability of NIH/3T3 was measured using a wound healing size tool from the ImageJ software. The images of the cells migrated and spread over the wound area were observed and photographed using a phase contrast inverted microscope at 0 h and 18 h. Scale bar = 500 μm. Corresponding bar graphs on the right column represent the percentage of cell-free area at a given time interval during the scratch wound assay. Statistical analysis was performed using the one-way ANOVA with Tukey's post hoc method, and the data are expressed as the mean ± SD; $n = 4$ per group (where, ##$p < 0.01$ compared with control (TCP) and AFC, **$p < 0.01$ compared with control and AC0 and ***$p < 0.001$ compared with AC0 and AF0 and $$$ $p < 0.001$).

Conclusion

We have reported the fabrication of alginate hydrogel microcapsules embedded with chitin nanofibrils and gelled with divalent and trivalent metal ions, using electrostatic encapsulation techniques. Rheological study confirmed that the Fe^{3+} crosslinked hydrogels exhibited higher shear and loss moduli as compared to their Ca^{2+} counterparts. The performance evaluation of alginate–chitin microcapsules crosslinked with divalent (*e.g.*, Ca^{2+}) and trivalent (*e.g.*, Fe^{3+}) metal ions demonstrates the impact of gelling agents on structural integrity, mechanical properties, and biological functionality. Among the

fabricated microcapsules, those gelled with Fe^{3+} (AF0) and a combination of Fe^{3+} and Ca^{2+} (AFC) outperformed Ca^{2+}-only gelled capsules (AC0) across multiple criteria. AF0 and AFC maintained superior structural stability under physiological conditions, resisting swelling and surface degradation over extended incubation in PBS. Biologically, all formulations supported NIH/3T3 cell viability above 75% over five days; however, AF0 microcapsules particularly promoted improved cell attachment, proliferation, and migration, as shown in morphological and scratch assay studies. These findings highlight the advantages of Fe^{3+}-gelled microcapsules in achieving both mechanical robustness and favorable biological interactions, underscoring their potential for applications in regenerative medicine, tissue engineering, and targeted cell delivery systems.

Materials and methods

Materials and reagents

Chitin flakes (C7170-100G), calcium chloride, and ferric chloride were purchased from Millipore Sigma, USA. Alginate (PRONOVA UP MVG) was obtained from Novamatrix, Industriveien 33 N-1337 Norway. Hanks' balanced salt solution (HBSS) buffer was obtained from Life Technology (Gaithersburg, MD, USA). Dulbecco modified eagle medium (DMEM), fetal bovine serum (FBS), penicillin–streptomycin, TritonX-100, AlamarBlue™ cell viability reagent were purchased from Thermo Fisher Scientific (Waltham, MA, USA). Likewise, trypsin, ethylenediaminetetraacetic acid (EDTA), 4′,6-diamidino-2-phenylindole (DAPI), lactate dehydrogenase (LDH) cytotoxicity assay kit were obtained from Invitrogen (Waltham, MA, USA). Acridine orange/propidium iodide (AOPI) was obtained from Fisher Scientific (Hampton, NH, USA). All the chemicals and reagents were of analytical grade and used as received without further purification.

Preparation of alginate–chitin nanofibril solution

Sodium alginate salt sterilized overnight in ultraviolet light was dissolved in Hank's balenced salt solution and stirred for 8 hours using magnetic stir bar to make 2% (w/v) solution. Likewise, chitin from shrimp shells was also sterilized in UV light before dispersion in sterilized deionized (DI) water to form a 2% (w/v) suspension. The suspension was then converted into nanofibrils using a defibrillation process described by Tanaka *et al.*[59] Briefly, 0.5 g of chitin was dispersed in 25 mL of DI water and sonicated under a nitrogen atmosphere in an ice bath for 3 hours to disentangle the chitin flakes into a nanofibril suspension. The resulting chitin fibrils were sterilized under UV light prior to mixing with alginate solution in the mass ratio of 60/40 (alginate/chitin) and subjected to bath sonication for 10 minutes to mix them homogeneously. The homogenously mixed alginate/chitin composite suspension was subsequently used for rheological studies, physicochemical characterization, and the fabrication of microcapsules.

Preparation of hydrogel and rheological studies

Hydrogel discs were prepared using a gelling bath of $CaCl_2$, $FeCl_3$, and a $CaCl_2$/$FeCl_3$ mixture from a 60/40 (w/w) composition of alginate 2% (w/v)/chitin 2% (w/v) suspension. Solutions of calcium chloride and ferric chloride at a concentration of 150 mM were prepared in sterilized deionized water; this concentration was selected based on previous research by other authors[60–62] and our own studies in preparation of alginate-based hydrogels.[63] For the gelling bath, 10 mL of $CaCl_2$ and $FeCl_3$ solutions each having 150 mM concentration were added into two separate wells, while a mixture containing 5 mL each of $CaCl_2$ and 5 mL of $FeCl_3$ solution was used in the third well of a six-well plate. 1 mL of a composite polymer prepared from mixing 600 μL of alginate solution 2% (w/v) and 400 μL chitin 2% (w/v) was carefully dropped into each gelling bath and left for 10 minutes to form a translucent hydrogel disc. Rheological property of the hydrogel discs was measured using an MCR 302 rheometer (Anton Paar, Austria). The hydrogel disc was positioned on the lower platform, and the upper stage of the rheometer, fitted with an 8 mm diameter beam, was lowered until it contacted the sample's surface. Excess material outside the beam was carefully removed, and the surrounding area was dabbed to eliminate any remaining liquid. The storage modulus (G') and loss modulus (G'') of the hydrogel were measured at 25 °C using a frequency sweep experiment, conducted over a frequency range of 0.1–100 Hz with a constant strain of 0.1%.

Fabrication of hydrogel microcapsules

Microcapsules of the alginate/chitin composite were fabricated using electrohydrodynamic atomization, also known as electrospray, under a voltage of 8 kV. The combined mixture of alginate and chitin prepared by mixing 600 μL of the alginate solution (2% w/v) with 400 μL chitin (2% w/v) nanofibrils suspension was vortexed for 5 minutes before using it for fabrication. The composite polymer solution was aspirated into a syringe fitted with a 24 gauge needle (Rame-Hart Instrument Co., Succasunna, NJ) and loaded onto a vertically mounted syringe pump. The polymer was slowly extruded at a flow rate of

Table 1 Summary of hydrogel samples fabricated in different gelling baths. For each microcapsule fabrication 600 μL of alginate solution 2% (w/v) was mixed with 400 μL chitin 2% (w/v)

Microcapsule name	Mass percentage of alginate and chitin fibril	$CaCl_2$ in gelling bath (mL)	$FeCl_3$ in gelling bath (mL)	Concentrations of the ions in the gelling bath (mM)
AC0	60 and 40	50	0	150 (Ca^{2+})
AF0	60 and 40	0	50	150 (Fe^{3+})
AFC	60 and 40	25	25	75 (Fe^{3+}) and 75 (Ca^{2+})

3 mL h^{-1} through the needle into separate beakers containing gelling baths of 150 mM $CaCl_2$, $FeCl_3$, and a $CaCl_2/FeCl_3$ mixture. An 8 kV voltage was applied to create an electric field, maintaining a 40 mm distance between the nozzle tip and the bath solution during microcapsule fabrication. The microcapsules were allowed to gel for 10 minutes; then rinsed with DI water to remove excess gelling solutions before further characterization. Fabricated microcapsules were dispersed in DI water, cell media, and PBS solution and incubated for 4 days at 37 °C and 5% CO_2 before characterizing for morphology, size, and stability. Table 1 shows the volumetric composition of alginate, chitin as well as gelling bath of calcium chloride and ferric chloride with their respective concentration during fabrication of microcapsules.

Analysis of chemical composition of hydrogel

Hydrogel samples of the alginate/chitin prepared as described in above section were washed with DI water multiple times to remove excess unreacted gelling agents. The resulting hydrogel was frozen and freeze-dried in a Labron Free Zone freeze dryer (New Life Scientific, Ohio, USA) for 24 h at a chamber pressure of 0.01 millibar and temperature of −80 °C. Fourier-transform infrared (FTIR) spectra of the dried hydrogel samples were then recorded using an FTIR spectrometer (Shimadzu IR-100, Tokyo, Japan) in the range of 500–4000 cm^{-1} with a resolution of 2 cm^{-1} over 20 scans per spectrum. The crystallinity of each dried hydrogel sample was analyzed using a benchtop X-ray diffractometer (Rigaku Miniflex600, Tokyo, Japan). The instrument operated in continuous mode with increments of 10° min^{-1} and scanned over a 2θ range of 10° to 90°. Monochromatic Cu Kα radiation (1.542 Å) was used, and samples were analyzed between 10° and 60° (2θ). The voltage and current were set at 30 kV and 30 mA, respectively.

Characterization of hydrogel microcapsules

Morphology and size distribution. The morphology of chitin-embedded alginate microcapsules (AC0, AF0, and AFC) was studied using an inverted optical microscope (EVOS® FL Core Digital Inverted). Optical images were taken while microcapsules were in cell culture conditions, and their size distribution was assessed using ImageJ software (NIH, USA). Freeze-dried microcapsules were gold-coated using a Polaron E 5400 sputter coater, and surface morphology was visualized with SEM (JEOL, Japan) at an accelerating voltage of 10 kV and 10 μA current. Additionally, elemental quantification of these lyophilized microcapsules was analyzed by Energy Dispersive X-ray technique.

Mechanical properties

The stiffness of microcapsules was analyzed by applying compressive force between two parallel plates to each microcapsule using a Micro-Tester (Cell Scale Biomaterial Testing, Waterloo, Canada) according to prior publication.[49] Briefly, a circular tungsten microbeam with a length of 58 mm and diameter of 0.5588 mm was used to apply a constant force to hydrogel microspheres ($n = 5$). Microcapsule submersed in DI water for 24 h was placed on the bottom stationary plate then sandwiched by moving the top plate, in water bath at room temperature. Hydrogel microcapsules were compressed to 30% of their original diameter for 30 seconds of loading and recovery time. The force and displacement were measured using the incorporated image analysis module in the microscale system. Force *vs.* displacement and displacement *vs.* time curves were generated using the company software, UniVert, version 1.0.0.1. The Young's modulus of the microcapsules was calculated from the raw data.

Fabrication of cell-encapsulated microcapsules

Mouse fibroblast cells (NIH/3T3, ATCC Cell Line Bank 1658, Manassas, VA, USA) were cultured in standard Dulbecco Modified Eagle Medium (DMEM) supplemented with 10% FBS and 1% penicillin/streptomycin. Cells were grown in 75 cm^2 tissue culture flasks at 37 °C in a 5% CO_2 humidified environment. At 80% confluency, cells were dissociated with 0.25% trypsin/EDTA, collected, and centrifuged. The pellets were resuspended in a fresh medium to the desired cell density.

NIH/3T3 cells at a density of 1×10^6 mL^{-1} in cell culture media were suspended with UV sterilized 1 mL of alginate/chitin (60/40) (w/w) and electrosprayed under the same conditions as described in fabrication of microcapsules. Cell-encapsulated microcapsules (AC0, AF0, and AFC) were washed three times at 5-minute intervals in Hanks' balanced salt solution (1X), transferred to complete cell culture media (DMEM) in 24-well plates, and incubated at 37 °C in a humidified atmosphere with 5% CO_2. Culture media was changed with fresh media every 2 days. For the indirect cell culture study, each set of microcapsules fabricated as outlined in previous section was immersed in 4 mL of fresh medium in three separate 15 mL centrifuge tubes, and incubated at 37 °C in a humidified environment with 5% CO_2 for 24 h. After incubation, the culture medium was carefully aspirated from each tube and used for the indirect cell culture study with the NIH3/T3 cells. The cells were seeded in 48-well plates at a density of 3×10^4 cells per well, using the extracted medium. Freshly prepared media served as the control for each cell culture study. The plates were incubated at 37 °C in a 5% CO_2 atmosphere. Live and dead cell staining, along with the morphology of NIH/3T3 cells in indirect contact, were assessed using the fluorescence dye, acridine orange/propidium iodide (AOPI).

Lactate dehydrogenase assay

The LDH assay was conducted using CyQUANT™ LDH cytotoxicity assay kit to assess the toxicity of the different microcapsule samples (AC0, AF0, and AFC) on the cells. Media from the cultured cell-microcapsules were collected at various time intervals and preserved at 4 °C for further experiments. Briefly, 50 μL of the collected cultured media from the cell-encapsulated microcapsules was transferred to the wells of flat bottom 96-well plates in triplicate. Then, 50 μL of the reaction mixture was added to each well, and the plates were incubated in the dark for 30 minutes at room temperature. The reaction was stopped by adding 50 μL of stop solution to each

well, and gently mixed by tapping. The absorbance of the reaction assay solution was measured at 490 nm using 570 nm as a reference wavelength using a microplate reader (Clariostar Plus, BMG LABTECH Inc., Cary, NC, USA) to calculate the cytotoxicity of the microcapsules on 1, and 5 days.

Alamar blue assay

Cell viability was measured using the AlamarBlue assay kit following the manufacturer's standard protocol. Briefly, 100 μL culture media from cell-encapsulated microcapsules were collected and transferred into wells of 96-well plates ($n = 6$). Then, 10% AlamarBlue was added and incubated for 4 hours at 37 °C in a 5% CO_2 humidified incubator. The absorbance of the AlamarBlue reaction solution was measured with a microplate reader (Clariostar Plus, BMG LABTECH Inc., Cary, NC, USA) at 570 nm using 600 nm as a reference wavelength. The cell viability percentage was calculated following the manufacturer's standard protocol.

Fluorescence imaging and analysis

The viability studies of cells encapsulated in microcapsules were conducted during different culture periods (1, and 5 days). The cells were stained with AOPI stain to examine the live and dead cells following the manufacturer's protocol. Briefly, the media from the cell-encapsulated microcapsule cultured well plates were carefully aspirated, and the microcapsules were rinsed with PBS three times. Then, the working solution of AOPI was added to each well and incubated at 37 °C for 10 minutes. Fluorescence z-stack images of the stained microcapsules were captured using an Olympus IX83 microscope with Olympus cellSens Dimension software (Olympus Corporation, Shinjuku, Tokyo, Japan). Live cells stained green and dead cells-stained red. Cell counts for live and dead cells were determined from the fluorescence images using ImageJ 1.53c software (NIH, Bethesda, MD, USA). A similar procedure was followed to stain and capture fluorescence images of cells grown in extracted media from different microcapsules to study cell viability using the Olympus microscope.

Cell morphology studies

The morphology of the cells cultured in extracted media and those in encapsulated microcapsules was examined by staining with ActinRed™ ReadyProbe™ Reagent (rhodamine-phalloidin) and DAPI (4′,6-diamidino-2-phenylindole), to visualize actin filaments and cell nuclei. The morphology of cells grown for 1 and 5 days in the extracted media of microcapsules, TCP as control media, and cells encapsulated in different microcapsules (AC0, AF0, and AFC) were examined. The cells and encapsulated microcapsules were washed with PBS and fixed with a 4% paraformaldehyde solution for 10 minutes. The fixed cells were permeabilized with 0.2% Triton X-100 for 2 minutes at room temperature. Subsequently, 1% bovine serum albumin (BSA) was used to block the permeabilized cells for 30 minutes at room temperature. Then, cells and cells encapsulated microcapsules were stained with rhodamine-phalloidin for 20 minutes at RT in dark to visualize cytoplasm and with DAPI for 5 minutes at RT in dark to visualize nuclei. Fluorescence images of the stained cells were captured using an Olympus 1X83 microscope.

Cell migration assay

Cell migration assay with NIH/3T3 cell cultures was used to determine if the different microcapsules could promote wound closure *in vitro*. Briefly, the cells were seeded within 24-well plates with a complete medium at a density of 1.5×10^5 cells per well and allowed to grow to form a confluent monolayer. After 80% confluency, the cell sheet was wounded through scratching the culture well surface with a sterile 200 μL pipette tip. Then, the detached or fragment cells were washed with PBS and incubated with extracted media from different microspheres (AC0, AF0, and AFC) that were immersed in complete media for 24 h, a freshly prepared complete medium was used as a control. The cell migration was monitored and photographed under a phase contrast inverted microscope at 0 h and 18 h to measure cell-free area. After that, the percentage of cell-free area was measured and quantified using a wound healing size tool from ImageJ Software.

Statistical analysis

Data were analyzed for significance using OriginPro software (OriginLab, Northampton, MA, USA) through one-way analysis of variance (ANOVA). All results were expressed as mean ± S.D., A post hoc Tukey's test was performed with ANOVA for multiple comparisons. The α-value was set to 0.05, and p-values of less than 0.05 were considered statistically significant.

Data availability

All data generated in this study will be made available by the corresponding author on reasonable request.

Author contributions

Conceptualization, N. B.; methodology, T. S., S. S.; writing—original draft, T. S.; writing—review & editing, B. P. R. and N. B.; formal analysis, B. P. R., T. S. and N. B.; project administration, N. B. All authors have read and agreed to the published version of the manuscript.

Conflicts of interest

There are no conflicts to declare.

Acknowledgements

This work was supported financially by the National Science Foundation-Excellence in Research (NSF-EiR 2100861). Part of this research work was also supported by Engineering Research Center for Hybrid Autonomous Manufacturing Moving from Evolution to Revolution (ERC – HAMMER, EEC-2133630) and NSF Engines: Piedmont Triad Regenerative Medicine Engine (NSF-2315654). We thank Bishnu Kumar Shrestha, Reedwan Bin

Zafar Auniq, Milani Needam and Felix Tettey for their technical assistance in research. Characterization of the scaffolds was performed in part at the Joint School of Nanoscience and Nanoengineering (SENIC-NNCI) at North Carolina A&T State University, which is supported by the National Science Foundation (NSF ECCS-1542174) and facilities of the College of Engineering.

References

1 M. Mobaraki, M. Ghaffari, and M. Mozafari, Self-healing polymers for composite structural applications, in *Self-healing Composite Materials*, Elsevier, 2020, pp. 33–51.
2 T. Andersen, P. Auk-Emblem and M. Dornish, 3D cell culture in alginate hydrogels, *Microarrays*, 2015, **4**(2), 133–161.
3 X. Li, B. Cho, R. Martin, *et al.*, Nanofiber-hydrogel composite–mediated angiogenesis for soft tissue reconstruction, *Sci. Transl. Med.*, 2019, **11**(490), eaau6210.
4 S. Khanal, S. R. Bhattarai, J. Sankar, R. K. Bhandari, J. M. Macdonald and N. Bhattarai, Nano-fibre integrated microcapsules: A nano-in-micro platform for 3D cell culture (vol 13, 1269, 2023), *Sci. Rep.*, 2019, **9**(1), 13951.
5 M. R. Dethe, A. Prabakaran, H. Ahmed, M. Agrawal, U. Roy and A. Alexander, PCL-PEG copolymer based injectable thermosensitive hydrogels, *J. Controlled Release*, 2022, **343**, 217–236.
6 S. L. Tomić, M. M. Mićić, S. N. Dobić, J. M. Filipović and E. H. Suljovrujić, Smart poly (2-hydroxyethyl methacrylate/itaconic acid) hydrogels for biomedical application, *Radiat. Phys. Chem.*, 2010, **79**(5), 643–649.
7 Y. Tsai, C. Chang and Y. Yeh, Formation of highly elastomeric and property-tailorable poly (glycerol sebacate)-co-poly (ethylene glycol) hydrogels through thiol–norbornene photochemistry, *Biomater. Sci.*, 2020, **8**(17), 4728–4738.
8 A. S. Hoffman, Hydrogels for biomedical applications, *Adv. Drug Delivery Rev.*, 2012, **64**, 18–23.
9 P. P. Phatchayawat, A. Khamkeaw, S. Yodmuang and M. Phisalaphong, 3D bacterial cellulose-chitosan-alginate-gelatin hydrogel scaffold for cartilage tissue engineering, *Biochem. Eng. J.*, 2022, **184**, 108476.
10 W. G. Herrick, T. V. Nguyen, M. Sleiman, S. McRae, T. S. Emrick and S. R. Peyton, PEG-phosphorylcholine hydrogels as tunable and versatile platforms for mechanobiology, *Biomacromolecules*, 2013, **14**(7), 2294–2304.
11 B. J. Gill, D. L. Gibbons, L. C. Roudsari, *et al.*, A synthetic matrix with independently tunable biochemistry and mechanical properties to study epithelial morphogenesis and EMT in a lung adenocarcinoma model, *Cancer Res.*, 2012, **72**(22), 6013–6023.
12 T. R. Kyriakides, H. Kim, C. Zheng, L. Harkins, W. Tao and E. Deschenes, Foreign body response to synthetic polymer biomaterials and the role of adaptive immunity, *Biomed. Mater.*, 2022, **17**(2), 022007.
13 J. M. Anderson, A. Rodriguez and D. T. Chang, Foreign body reaction to biomaterials, *Semin. Immunol.*, 2008, **20**(2), 86–100.
14 P. Baharlouei and A. Rahman, Chitin and chitosan: Prospective biomedical applications in drug delivery, cancer treatment, and wound healing, *Mar. Drugs*, 2022, **20**(7), 460.
15 G. A. Kazi and O. Yamamoto, Effectiveness of the sodium alginate as surgical sealant materials, *Wound Medicine*, 2019, **24**(1), 18–23.
16 Q. Cong, F. Xiao, W. Liao, Q. Dong and K. Ding, Structure and biological activities of an alginate from sargassum fusiforme, and its sulfated derivative, *Int. J. Biol. Macromol.*, 2014, **69**, 252–259.
17 G. T. Grant, E. R. Morris, D. A. Rees, P. J. C. Smith and D. Thom, Biological interactions between polysaccharides and divalent cations: The egg-box model, *FEBS Lett.*, 1973, **32**(1), 195–198.
18 Y. Dong, W. Dong, Y. Cao, Z. Han and Z. Ding, Preparation and catalytic activity of fe alginate gel beads for oxidative degradation of azo dyes under visible light irradiation, *Catal. Today*, 2011, **175**(1), 346–355.
19 J. P. Frampton, M. R. Hynd, M. L. Shuler and W. Shain, Fabrication and optimization of alginate hydrogel constructs for use in 3D neural cell culture, *Biomed. Mater.*, 2011, **6**(1), 015002.
20 S. J. Bidarra, C. C. Barrias, K. B. Fonseca, M. A. Barbosa, R. A. Soares and P. L. Granja, Injectable *in situ* crosslinkable RGD-modified alginate matrix for endothelial cells delivery, *Biomaterials*, 2011, **32**(31), 7897–7904.
21 T. Boontheekul, H. Kong and D. J. Mooney, Controlling alginate gel degradation utilizing partial oxidation and bimodal molecular weight distribution, *Biomaterials*, 2005, **26**(15), 2455–2465.
22 Y. Huang, M. Yao, X. Zheng, *et al.*, Effects of chitin whiskers on physical properties and osteoblast culture of alginate based nanocomposite hydrogels, *Biomacromolecules*, 2015, **16**(11), 3499–3507.
23 H. K. Noh, S. W. Lee, J. Kim, *et al.*, Electrospinning of chitin nanofibers: Degradation behavior and cellular response to normal human keratinocytes and fibroblasts, *Biomaterials*, 2006, **27**(21), 3934–3944.
24 Y. Cao, X. Shen, Y. Chen, J. Guo, Q. Chen and X. Jiang, pH-induced self-assembly and capsules of sodium alginate, *Biomacromolecules*, 2005, **6**(4), 2189–2196.
25 V. Florián-Algarín and A. Acevedo, Rheology and thermotropic gelation of aqueous sodium alginate solutions, *J. Pharm. Innov.*, 2010, **5**(1), 37–44.
26 S. A. P. Siboro, D. S. B. Anugrah, K. Ramesh, S. Park, H. Kim and K. T. Lim, Tunable porosity of covalently crosslinked alginate-based hydrogels and its significance in drug release behavior, *Carbohydr. Polym.*, 2021, **260**, 117779.
27 M. Park, D. Lee and J. Hyun, Nanocellulose-alginate hydrogel for cell encapsulation, *Carbohydr. Polym.*, 2015, **116**, 223–228.
28 P. Tordi, F. Ridi, P. Samorì and M. Bonini, Cation-Alginate complexes and their hydrogels: A powerful toolkit for the

development of Next-Generation sustainable functional materials, *Adv. Funct. Mater.*, 2025, **35**(9), 2416390.
29 S. K. Bajpai and S. Sharma, Investigation of swelling/degradation behaviour of alginate beads crosslinked with Ca2 and Ba2 ions, *React. Funct. Polym.*, 2004, **59**(2), 129–140.
30 K. J. Sreeram, H. Yamini Shrivastava and B. U. Nair, Studies on the nature of interaction of iron(III) with alginates, *Biochim. Biophys. Acta, Gen. Subj.*, 2004, **1670**(2), 121–125.
31 C. Menakbi, F. Quignard and T. Mineva, Complexation of trivalent metal cations to mannuronate type alginate models from a density functional study, *J. Phys. Chem. B*, 2016, **120**(15), 3615–3623.
32 P. N. Dave, P. M. Macwan and B. Kamaliya, Synthesis and rheological investigations of gum-ghatti-cl-poly (NIPA-co-AA)-graphene oxide based hydrogels, *Mater. Adv.*, 2023, **4**(14), 2971–2980.
33 J. Gong, L. Wang, J. Wu, *et al.*, The rheological and physicochemical properties of a novel thermosensitive hydrogel based on konjac glucomannan/gum tragacanth, *LWT–Food Sci. Technol.*, 2019, **100**, 271–277.
34 M. H. Chen, L. L. Wang, J. J. Chung, Y. Kim, P. Atluri and J. A. Burdick, Methods to assess shear-thinning hydrogels for application as injectable biomaterials, *ACS Biomater. Sci. Eng.*, 2017, **3**(12), 3146–3160.
35 A. C. Gaffey, M. H. Chen, C. M. Venkataraman, *et al.*, Injectable shear-thinning hydrogels used to deliver endothelial progenitor cells, enhance cell engraftment, and improve ischemic myocardium, *J. Thorac. Cardiovasc. Surg.*, 2015, **150**(5), 1268–1277.
36 G. Stojkov, Z. Niyazov, F. Picchioni and R. K. Bose, Relationship between structure and rheology of hydrogels for various applications, *Gels*, 2021, **7**(4), 255.
37 Y. Wang, Y. Zhao, J. He, *et al.*, Doubling growth of egg-box structure during calcium-mediated molecular assembly of alginate, *J. Colloid Interface Sci.*, 2023, **634**, 747–756.
38 H. Malektaj, A. D. Drozdov and J. deClaville Christiansen, Mechanical properties of alginate hydrogels cross-linked with multivalent cations, *Polymers*, 2023, **15**(14), 3012.
39 H. Daemi and M. Barikani, Synthesis and characterization of calcium alginate nanoparticles, sodium homopolymannuronate salt and its calcium nanoparticles, *Sci. Iran.*, 2012, **19**(6), 2023–2028.
40 S. Jana, M. K. Trivedi, R. M. Tallapragada, *et al.*, Characterization of physicochemical and thermal properties of chitosan and sodium alginate after biofield treatment, *Pharm. Anal. Acta*, 2015, **6**(10), 1000430.
41 Y. A. Hamdan, S. Elouali, N. Eladlani, B. Lefeuvre, H. Oudadesse and M. Rhazi, Investigation on akis granulifera (coleoptera, sahlberg, 1823) as a potential source of chitin and chitosan: Extraction, characterization and hydrogel formation, *Int. J. Biol. Macromol.*, 2023, **252**, 126292.
42 B.-B. Lee, P. Ravindra and E.-S. Chan, Size and shape of calcium alginate beads produced by extrusion dripping, *Chem. Eng. Technol.*, 2013, **36**(10), 1627–1642.
43 D. Zaeim, M. Sarabi-Jamab, B. Ghorani, R. Kadkhodaee and R. H. Tromp, Electrospray assisted fabrication of hydrogel microcapsules by single- and double-stage procedures for encapsulation of probiotics, *Food Bioprod. Process.*, 2017, **102**, 250–259.
44 Z. Mai, J. Chen, T. He, *et al.*, Electrospray biodegradable microcapsules loaded with curcumin for drug delivery systems with high bioactivity, *RSC Adv.*, 2017, **7**(3), 1724–1734.
45 A. S. Qayyum, E. Jain, G. Kolar, Y. Kim, S. A. Sell and S. P. Zustiak, Design of electrohydrodynamic sprayed polyethylene glycol hydrogel microspheres for cell encapsulation, *Biofabrication*, 2017, **9**(2), 025019.
46 K. J. Sreeram, H. Yamini Shrivastava and B. U. Nair, Studies on the nature of interaction of iron(III) with alginates, *Biochim. Biophys. Acta, Gen. Subj.*, 2004, **1670**(2), 121–125.
47 P. Agulhon, V. Markova, M. Robitzer, F. Quignard and T. Mineva, Structure of alginate gels: Interaction of diuronate units with divalent cations from density functional calculations, *Biomacromolecules*, 2012, **13**(6), 1899–1907.
48 S. Huang, P. Du, C. Min, Y. Liao, H. Sun and Y. Jiang, Poly (1-amino-5-chloroanthraquinone): Highly selective and ultrasensitive fluorescent chemosensor for ferric ion, *J. Fluoresc.*, 2013, **23**, 621–627.
49 T. Sapkota, B. K. Shrestha, S. Shrestha and N. Bhattarai, Chitin nanofibrils enabled Core–Shell microcapsules of alginate hydrogel, *Nanomaterials*, 2023, **13**(17), 2470.
50 T. Baudequin, H. Wee, Z. Cui and H. Ye, Towards ready-to-use iron-crosslinked alginate beads as mesenchymal stem cell carriers, *Bioengineering*, 2023, **10**(2), 163.
51 I. Machida-Sano, Y. Matsuda and H. Namiki, In vitro adhesion of human dermal fibroblasts on iron cross-linked alginate films, *Biomed. Mater.*, 2009, **4**(2), 025008.
52 B. M. Baker and C. S. Chen, Deconstructing the third dimension–how 3D culture microenvironments alter cellular cues, *J. Cell Sci.*, 2012, **125**(13), 3015–3024.
53 P. Semenyuk and V. Muronetz, Protein interaction with charged macromolecules: From model polymers to unfolded proteins and post-translational modifications, *Int. J. Mol. Sci.*, 2019, **20**(5), 1252.
54 S. D. Tatum, S. Saudi, F. Tettey, R. K. Bhandari and N. Bhattarai, Novel hydrogel-bronchial epithelial cell spheroids for toxicological evaluation, *Biomed. Sci. Instrum.*, 2021, **57**(4), 406–419.
55 G. Rishi and V. N. Subramaniam, The relationship between systemic iron homeostasis and erythropoiesis, *Biosci. Rep.*, 2017, **37**(6), BSR20170195.
56 J. Kantapan, N. Anukul, N. Leetrakool, G. Rolin, J. Vergote and N. Dechsupa, Iron–quercetin complex preconditioning of human peripheral blood mononuclear cells accelerates angiogenic and fibroblast migration: Implications for wound healing, *Int. J. Mol. Sci.*, 2021, **22**(16), 8851.
57 J. N. I. Balitaan, C. Hsiao, J. Yeh and K. S. Santiago, Innovation inspired by nature: Biocompatible self-healing injectable hydrogels based on modified-β-chitin for wound healing, *Int. J. Biol. Macromol.*, 2020, **162**, 723–736.
58 M. Sołtan, D. Bartusik-Aebisher and D. Aebisher, The potential of oxygen and nitrogen species-regulating drug

delivery systems in medicine, *Front. Bioeng. Biotechnol.*, 2022, **10**, 973080.

59 K. Tanaka, K. Yamamoto and J. Kadokawa, Facile nanofibrillation of chitin derivatives by gas bubbling and ultrasonic treatments in water, *Carbohydr. Res.*, 2014, **398**, 25–30.

60 R. E. Jeffries, M. P. Gamcsik, K. R. Keshari, *et al.*, Effect of oxygen concentration on viability and metabolism in a fluidized-bed bioartificial liver using 31P and 13C NMR spectroscopy, *Tissue Eng., Part C*, 2013, **19**(2), 93–100.

61 B. Y. Swamy and Y. S. Yun, In vitro release of metformin from iron (III) cross-linked alginate–carboxymethyl cellulose hydrogel beads, *Int. J. Biol. Macromol.*, 2015, **77**, 114–119.

62 Y. Zhai, X. Meng, H. Duan, Z. Ding, Y. Liu and L. Lucia, Super Stable and Tough Hydrogel Containing Covalent, Crystalline, and Ionic Cross-Links, *Macromol. Chem. Phys.*, 2016, **217**(1), 32–38.

63 S. Khanal, S. R. Bhattarai, J. Sankar, R. K. Bhandari, J. M. Macdonald and N. Bhattarai, Nano-fibre integrated microcapsules: A nano-in-micro platform for 3D cell culture, *Sci. Rep.*, 2019, **9**(1), 13951.